

## RUPRECHT 147: THE OLDEST NEARBY OPEN CLUSTER AS A NEW BENCHMARK FOR STELLAR ASTROPHYSICS

JASON L. CURTIS<sup>1,2,3</sup>, ANGIE WOLFGANG<sup>3,4</sup>, JASON T. WRIGHT<sup>1</sup>, JOHN M. BREWER<sup>5</sup>, AND JOHN ASHER JOHNSON<sup>6</sup>  
SUBMITTED TO AJ: *June 1, 2012*

### ABSTRACT

Ruprecht 147 is a hitherto unappreciated open cluster that holds great promise as a standard in fundamental stellar astrophysics. We have conducted a radial velocity survey of astrometric candidates with Lick, Palomar, and MMT observatories and have identified over 100 members, including 5 blue stragglers, 11 red giants, and 5 SB2 binaries. We estimate the cluster metallicity from spectroscopic analysis, using Spectroscopy Made Easy (SME), and find it to be  $[M/H] = +0.08 \pm 0.03$ . We have obtained deep CFHT/MegaCam  $g'r'i'z'$  photometry and fit Padova isochrones to the  $(g' - i')$  and 2MASS  $(J - K_s)$  CMDs, using the  $\tau^2$  maximum-likelihood procedure of Naylor (2009). We find best fits for isochrones at age  $t = 2.5 \pm 0.25$  Gyr,  $m - M = 7.35 \pm 0.1$ , and  $A_V = 0.25 \pm 0.05$ , with significant uncertainty from the unresolved binary population and possibility of differential extinction across this large cluster. Our preferred model does not simultaneously fit the main sequence turnoff and the red giant branch in the optical CMD. We investigate alternative solutions and find that an older, closer and less extinguished Padova model with age  $t = 3.5$  Gyr,  $m - M = 7.0$ , and  $A_V = 0.10$  appears to better match the overall optical CMD (particularly the red giant branch). We do not favor this model because it poorly fits the upper main sequence in the optical, the age is inconsistent with our spectroscopic results, and our preferred model better fits the NIR CMD. Still, we cannot yet conclusively rule out the older solution. At 250 – 300 pc and an age of 2.5 – 3.5 Gyr, Ruprecht 147 is by far the oldest nearby star cluster.

*Subject headings:* open clusters: general — open clusters: individual (Ruprecht 147)

### 1. INTRODUCTION

The observational foundations of stellar astrophysics are studies of the Sun and stellar clusters. A few “benchmark” clusters form the basis of our understanding of stellar evolution, and the effects of abundance, age, and mass on stars. When fully characterized with precise ages, distances and metallicities, these clusters become touchstones for similar stars in the field and test models of stellar evolution and structure.

Galactic gravitational tidal forces are effective at disrupting most Galactic clusters on a time scale of a few hundred Myr (Soderblom 2010), so most clusters tend to be relatively young. This is fortunate for studies of early stellar evolution and massive stars: for such work stellar astrophysicists have access to several nearby young clusters (e.g. Pleiades  $\sim 100 - 200$  Myr; Hyades and Praesepe  $\sim 700$  Myr).

Studies of the older cool stars (age  $\gtrsim 1$  Gyr) that typify the field must rely on rarer and thus more distant clusters. Studies of the typical rotation, activity level, and photometry of G, K and M dwarfs as a function of age and mass, such as the WIYN Open Cluster Survey (WOCS<sup>7</sup>), the Palomar Transient Factory

(PTF, Agüeros et al. 2011) and the *Kepler* Cluster Study (Meibom et al. 2011), investigate clusters with distances of 1 – 4 kpc. These larger distance moduli can make spectroscopic study of their low mass members extremely difficult.

Fortunately, Dias, Lépine, & Alessi (2001) and Kharchenko et al. (2005) used catalog data to identify Ruprecht 147 (R147 = NGC 6774), and estimated its age to be  $\sim 2.5$  Gyr at a distance of 175 – 270 pc, making R147 by far the oldest nearby cluster (e.g. WEBDA lists NGC 752 at 1.1 Gyr and 457 pc, Figure 1).

#### 1.1. Pre-2000 Literature

Despite its promising scientific potential due to the unique combination of its age and distance, and despite having a similar distance and size to Praesepe, R147 was completely overlooked by stellar astronomers until the works by Dias et al. and Kharchenko et al.. This is likely because its proximity makes R147 a very sparse cluster on the sky: there are only  $\sim 50$  members with  $V < 11$  and only  $\sim 10$  with  $V < 9$  spread over 5 square degrees. Its presence is also obscured by its location in the Galactic plane ( $-14^\circ < b < -12^\circ$ , in Sagittarius), and the fact that due to its age, it lacks the many bright A stars that made similarly nearby clusters so obvious, even to the astronomers of antiquity.

In fact, a complete pre-2000 bibliography of R147 consists almost exclusively of entries in various catalogues. R147 was originally discovered in 1830 by John Herschel (Herschel 1833), who labelled it GC 4481 (Herschel 1863), and described it as “a very large straggling space full of loose stars” (Archinal & Hynes 2003). Since then it has appeared with numerous designations in-

<sup>1</sup> Department of Astronomy & Astrophysics, The Pennsylvania State University, University Park, PA 16802, USA

<sup>2</sup> jcurtis@psu.edu

<sup>3</sup> NSF Graduate Research Fellow

<sup>4</sup> Department of Astronomy & Astrophysics, University of California, Santa Cruz, CA 95064, USA

<sup>5</sup> Department of Astronomy, Yale University, New Haven, CT 06511, USA

<sup>6</sup> Department of Astrophysics, California Institute of Technology, Pasadena, CA 91125, USA

<sup>7</sup> <http://www.astro.wisc.edu/wocs/>

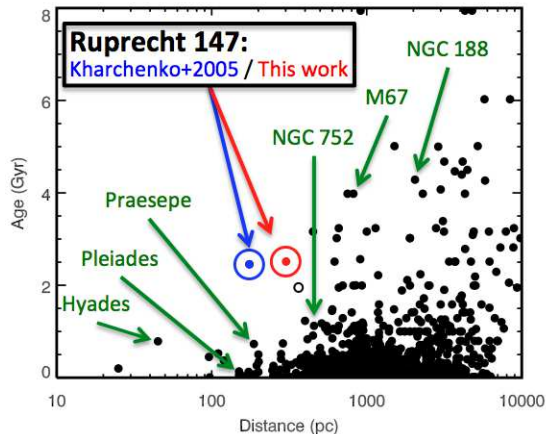


**Figure 1.** Data from the WEBDA database (Mermilliod & Paunzen 2003) showing all known clusters in distance – age space. R147 is by far the oldest nearby cluster, and holds great promise as a standard in fundamental stellar astrophysics: Kharchenko et al. (2005) values shown in blue, ours in red. WEBDA lists an age for M67 at 2.5 Gyr, but we plot it at 4 Gyr according to Pichardo et al. (2012) and references therein. The open circle next to R147 denotes Loden 1, with membership and properties determined by Kharchenko et al. (2005). They identify only nine  $1\text{-}\sigma$  members from proper motions and photometry, and none have measured radial velocities. The Loden 1 grouping has not been confirmed as a real open cluster, and the properties derived by the automated search of Kharchenko et al. (2005) are thus unreliable.

cluding NGC 6774, OCL 65, Lund 883 (Dreyer 1888; Alter, Ruprecht, & Vanysek 1958; Lynga & Palous 1987; Mermilliod 1995). Some star charts have even designated R147 as an asterism, and not a true cluster (e.g. “Burnham’s Celestial Handbook: An Observer’s Guide to the Universe Beyond the Solar System” lists NGC 6774 as “possibly not a true cluster” (Burnham 1966)). The name we use here originates from Ruprecht (1966), who classified R147 as a III-2-m cluster in the Trumpler system (Trumpler 1930, 160). According to Archinal & Hynes (2003), Brian Skiff realized that NGC 6774 and R147 are likely the same star cluster. Archinal & Hynes (2003) describe R147 as a “45’ sized V-shaped group of bright stars” that is “a sparse possible open cluster”, and estimate the cluster center as the location of HD 180228 (while this star’s photometry apparently places it on the R147 red giant branch, the proper motions from Tycho-2 ( $-1.6, -6.3$  mas/yr) and UCAC-3 ( $-3.5, -4.0$  mas/yr) are inconsistent with cluster membership). Figure 2 highlights our high-confidence members on an optical image. Herschel’s cluster identification is truly amazing, given the lack of a well defined cluster core. But those arguing for the asterism status were not entirely wrong either: of the 51 NOMAD stars with  $V < 9$  within  $\approx 2^\circ$  of the cluster center, only 11 are members.

## 1.2. Recent Work in the Literature

Only in the last decade has R147 received any individual attention in studies of open clusters. Dias, Lépine, & Alessi (2001) first identified R147’s membership based on the stellar population’s common proper motion: selecting stars in the Tycho-2 Catalogue (Høg et al. 2000) that were spatially coincident with BDA clusters (The Open Cluster DataBase, Mermilliod

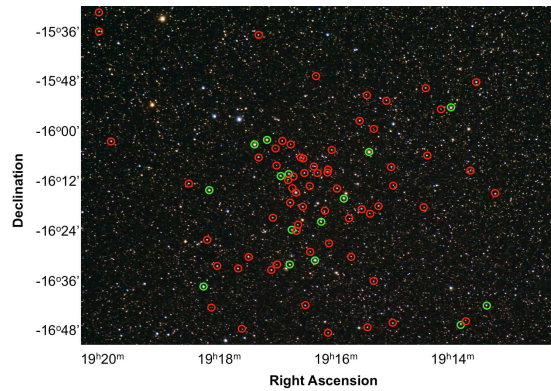


**Figure 2.** This astrophotograph of a portion of the Ruprecht 147 field was taken and kindly provided by Chris Beckett and Stefano Meneguolo of the Royal Astronomical Society of Canada. We have attached an approximate coordinate system solution (we have not solved for the field distortions) and circled the 80 high-confidence members in red. There are 52 stars in this image with  $V < 10$ , and only 17 are members of R147 and are circled green. Of the 52 NOMAD stars with  $V < 9$  within  $\approx 2^\circ$  of the cluster center, only 11 are members. It is remarkable that Herschel correctly identified this as an open cluster in 1830.

1995), they determined cluster membership with the Tycho-2 proper motions using the statistical method of Sanders (1971) and found 33 stars with mean proper motion of  $\mu_\alpha = -0.8 \pm 2.3$  and  $\mu_\delta = -28.5 \pm 2.3$  mas/yr. Dias, Lépine, & Alessi (2001) also provided the first distance estimate based on the only two available Hipparcos parallax measurements (HIP1, Perryman & ESA 1997):  $\pi = 3.57 \pm 1.01$  mas ( $280 \pm 79$  pc) for HIP 94635 (CWW 1)<sup>8</sup>, and  $3.75 \pm 1.04$  mas ( $267 \pm 74$  pc) for HIP 94803 (CWW 2), which they average to  $3.7 \pm 0.2$  mas, estimating the distance to R147 to be 250 pc<sup>9</sup>. Since then, van Leeuwen (2007a) (HIP2) has performed a new data reduction and issued an updated catalog with parallaxes of  $5.48 \pm 0.65$  mas ( $182 \pm 22$  pc) for HIP 94635, and  $4.92 \pm 0.79$  mas ( $203 \pm 33$  pc) for HIP 94803<sup>10</sup>.

Dias et al. (2002) compiled all available data for 2095 galactic clusters (*The New Catalogue of Optically Visible Open Clusters and Candidates*, or DAML02) and published an updated membership list and cluster properties for R147: 25 members, proper motion  $\mu_\alpha = -0.9 \pm 0.3$  and  $\mu_\delta = -29.3 \pm 0.3$  mas/yr,  $RV = 41$  km s<sup>-1</sup> (from the single published measurement in Wilson (1953), see Section 3.1), distance = 200 pc, color excess  $E(B - V) = 0.2$  mag., and an age 3.2 Myr (presumably from misidentifying blue stragglers as main sequence turnoff stars). Dias et al. re-classified R147 as IV-2-p (Trumpler system).

Following their 2002 work, Dias et al. (2006) se-

<sup>8</sup> Throughout this paper, we will refer to individual stars with the designation “CWW #” (CWW = Curtis, Wolfgang and Wright). Our membership list provides 2MASS IDs, astrometry, photometry, radial velocities, and membership probabilities for 108 stars. The CWW ID numbers sort these stars according to  $V$  magnitude (see Table 6).

<sup>9</sup> though this is clearly a numerical rounding error as  $1000 / 3.7 = 270$ , not 250.

<sup>10</sup> van Leeuwen (2007b, §3.3.1, 3.3.2) cautions against deriving distances and distance moduli from parallaxes when the relative error is greater than 10%. The Lutz – Kelker bias can also introduce a 0.1 magnitude systematic offset at 10% relative error.

lected all clusters in their DAML02 catalogue with known distances and queried the UCAC-2 catalogue (Zacharias et al. 2004b) for all stars within the measured cluster radii, plus  $2'$ , of their tabulated cluster centers. Employing similar methods as Dias, Lépine, & Alessi (2001), they derived a mean proper motion for R147 of  $\mu_\alpha = -4.62 \pm 0.37$  and  $\mu_\delta = -5.6 \pm 0.37$ , and identified 200 cluster members. Figure 3 shows the proper motions for stars in the R147 field, color-shaded by membership probability as derived by Dias et al. (2006). The black circle highlights the proper motion of R147 according to Kharchenko et al. (2005) and confirmed in this work, and shows that the Dias algorithm missed the cluster, locating the field stars instead. The Dias et al. (2006) membership list and cluster parameters are thus unreliable. Dias et al. (2006) attribute their algorithm’s failure to the large angular size of R147.

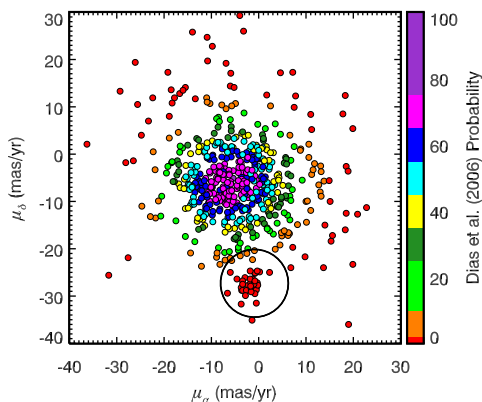


**Figure 3.** Proper motion diagram of stars in the R147 field, color shaded by membership probability as derived by Dias et al. (2006). The black circle highlights the proper motion of R147 (Kharchenko et al. 2005, and confirmed here). The Dias membership probabilities are clearly in error.

A similar automated effort has been undertaken by Kharchenko (2001), who assembled the All-Sky Compiled Catalogue of 2.5 Million Stars (ASCC-2.5), including proper motions from the Tycho-2 catalog (Høg et al. 2000), Johnson BV photometry, and radial velocities and spectral types when they are available. Kharchenko et al. (2005) searched this catalog and identified 520 Galactic open clusters, including R147. Their algorithm determined the core and cluster angular radii, and the distances, mean space motions (proper motion and radial velocity), and ages of the clusters. Three important differences exist between the Dias et al. (2006) membership and properties and those of Kharchenko et al. (2005): (1) Kharchenko et al. correctly identify the cluster, cataloging 41  $1\text{-}\sigma$  members; (2) they provide the first reliable age estimate of 2.45 Gyr from their isochrone fitting; and (3) they claim a new distance of only 175 pc, 75 pc closer than that inferred from the original Hipparcos parallaxes, but similar to the distances derived in HIP2. While we determine a similar age of  $\sim 2.5$  Gyr, we derive a distance  $d \approx 300$  pc (§4.3, 4.4) by fitting isochrones to a spectroscopically derived  $T_{\text{eff}} - \log g$  diagram, and

2MASS ( $J - K_S$ ) and CFHT/MegaCam ( $g' - i'$ ) color – magnitude diagrams. Figure 4 plots the CMD used by Kharchenko et al. (2005) to derive age and distance. The Tycho-2  $BV$  photometry is magnitude limited at  $V \sim 11$ , near the R147 main sequence turnoff. ASCC-2.5 is supplemented with various ground based photometry for fainter magnitudes, which Figure 4 demonstrates is insufficient for main sequence fitting. While the MSTO provides a strong constraint on the age, the discrepancy between our derived distance and that of Kharchenko et al. can be explained by the ill-defined ( $B - V$ ) main sequence. Their analysis was also hindered by a lack of a spectroscopically determined composition, and they assumed Solar metallicity. Without an accurate metallicity, and with a main sequence dominated by photometric error, it is difficult to disentangle visual extinction, age, composition and distance. Instead, Kharchenko et al. (2005) assumed  $A_V = 0.465$  from the Schlegel, Finkbeiner, & Davis (1998) dust map at their location for the cluster center, even though according to this dust map  $A_V$  varies from 0.3 to 0.6 mag. across the cluster (see §4.1). In Schilbach et al. (2006), Ruprecht 147 is for the first time specifically identified in a peer reviewed publication as an old nearby cluster<sup>11</sup>.

Despite these issues, the works of Dias, Lépine, & Alessi and Kharchenko et al. are significant because they essentially re-discovered Ruprecht 147 and provided the first good evidence that R147 is in fact the oldest nearby star cluster.

Most recently, Pakhomov et al. (2009) observed three cluster red giants and spectroscopically measured radial velocities and stellar properties (discussed in §3.1, 4.2). They determined the cluster metallicity to be super-Solar, thereby decreasing the estimated age, from a fit to an enriched Padova isochrone, to  $\sim 1.25$  Gyr, and derived a distance of  $280 \pm 100$  pc, along with a color excess of  $E(B - V) = 0.11$  (or  $A_V = 0.34$ , assuming  $R_V = 3.1$ ).

Ruprecht 147 has also appeared in the open cluster luminosity function study of Elsanhoury et al. (2011) and a paper on Galactic kinematics and structure as defined by open clusters by Zhu (2009), but these works undoubtedly suffer from a poorly determined membership and uncertain cluster properties.

We have begun an observational campaign to characterize R147, catalog its members, and prove its benchmark status. Here we present our initial efforts, detailing in particular our comprehensive R147 membership search that more than doubles the number of known cluster members (§3), and our derivation of the cluster’s age, distance, and metallicity (§4). We begin with an overview of our photometric and spectroscopic datasets.

## 2. OBSERVATIONAL DATASETS

Cluster members are identified by their common space motion, determined from proper motions and radial velocities, and by their placement on a color – magnitude diagram (CMD). We utilize the NOMAD and UCAC-3 astrometric catalogs for proper motions. We have high resolution, single order echelle spectra from MMT Obser-

<sup>11</sup> Although they incorrectly claim that they were first to determine the distance. As stated previously, Dias, Lépine, & Alessi (2001) recognized that two red giants with HIP parallaxes are members of R147 and averaged these measurements to find a distance of 250 pc.

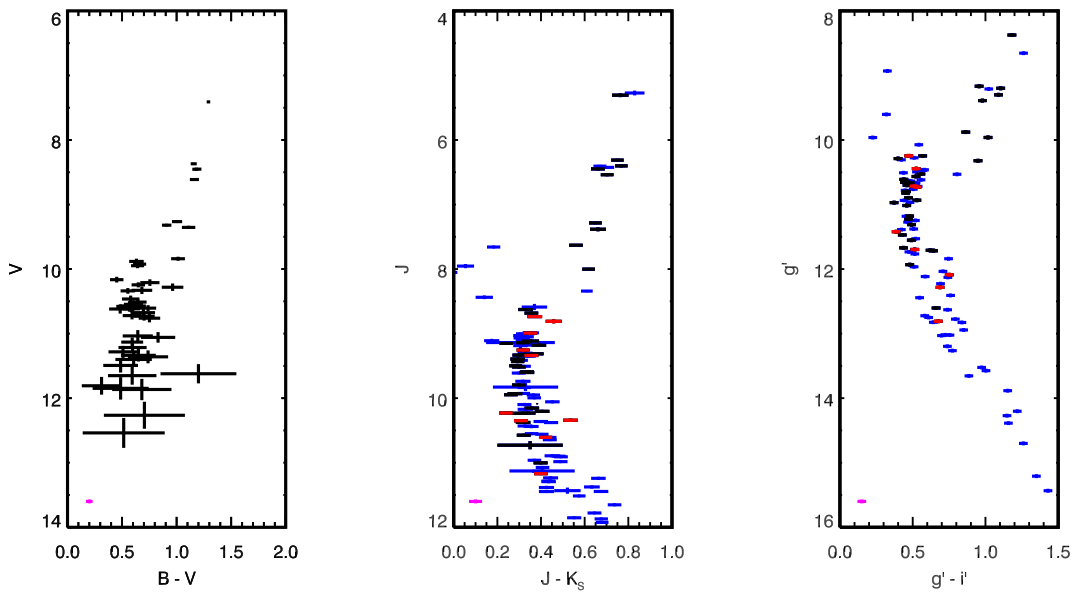


**Figure 4.** Ruprecht 147 color – magnitude diagrams. The left panel shows the  $BV$  photometry used by Kharchenko et al. (2005) to estimate age and distance by isochrone fitting. The main sequence is better defined in the 2MASS NIR CMD (center panel) and in our optical CMD (right panel), which explains the  $\approx 80\%$  discrepancy between the Kharchenko et al. distance of 175 pc and our value of  $\approx 300$  pc. The magenta symbol plotted in the lower left of each panel shows error bars at  $\sigma = 0.03$  mag. in each dimension for reference. Left Panel: The  $1-\sigma$  members of Kharchenko et al. (2005) on the  $(B - V)$  CMD. The Central and Right panels plot the same Kharchenko et al. in black, except for 10 in red which we do not consider members in this work. Our additional 72 members are plotted in blue. The central panel displays the 2MASS photometry and errors ( $\sigma_{(J-K_S)} = \sqrt{\sigma_J^2 + \sigma_{K_S}^2}$ ). The right panel presents our CFHT/MegaCam optical photometry, with errors in each dimension generously set at  $\sigma = 0.03$  mag.

vatory; high-resolution, cross-dispersed echelle spectra from Lick, Palomar, and Keck Observatories; and have acquired deep  $g'r'i'z'$  photometry of a 4 square degree field with CFHT/MegaCam. Other observing projects are underway, including deep NIR imaging with UKIRT (PI Adam Kraus), a 250 ks exposure of the cluster core with *Chandra* (PI Steve Saar), and an RV survey for K and M dwarf members with Magellan/MIKE (PI Steve Saar).

### 2.1. Astrometric Catalogs

Our initial list of candidate members is drawn from the NOMAD and UCAC-3 catalogs. The Naval Observatory Merged Astrometric Dataset (NOMAD, Zacharias et al. 2004a) combines data (positions, proper motions, and  $BVR/JHK$  photometry) for over 1 billion stars from the Hipparcos (Perryman & ESA 1997), Tycho-2, UCAC-2 (Zacharias et al. 2004b), USNO-B1, and 2MASS (Skrutskie et al. 2006) catalogues. The Third USNO CCD Astrograph Catalog (UCAC-3, Zacharias et al. 2009) expands on NOMAD by improving UCAC-2 in many ways, including complete sky coverage, reduced systematic errors for CCD observations, deeper photometry ( $R \approx 8 - 16$ ) for  $\sim 80$  million stars, and improved astrometry (resolved double stars, inclusion of several new catalogs, and re-reduction of early epoch photographic plates to derive proper motions). For each star, we use whichever catalog lists the smallest uncertainty in proper motion.

Dr. Adam Kraus has derived proper motions for the R147 field by incorporating 2MASS astrometry (private communication; method described in Kraus & Hillenbrand 2007). Two of our stars have measurements from his pipeline with smaller uncertainties than UCAC-3, and we adopt these values here (see Table 6).

### 2.2. Lick 3-m and Palomar 200-in Spectra and Radial Velocities

We performed initial radial velocity confirmation of suspected members to verify the existence of the cluster with the Hamilton echelle spectrometer on the 120 inch Shane telescope at Lick Observatory ( $R \sim 50,000$ ; Vogt 1987). Our strategy was to obtain RVs of known and suspected members, to identify new members, and to obtain high resolution spectra of the brightest members at high signal-to-noise ratios (SNR) for more detailed analysis of abundances and chromospheric activity.

We observed candidate cluster members on UT 2007 July 31 – August 1 and 2007 August 22 – 23, including the members identified by Kharchenko et al. (2005). To locate additional candidate members, we selected stars from the NOMAD catalog that were within  $1^\circ.25$  of the published cluster center and that had UCAC-2 and TYCHO-2 proper motions within 5 mas/yr of the Kharchenko et al. value. Although there are over 750,000 NOMAD stars in the field due to its large size and location in the Galactic plane, the cluster is separated enough from the field in proper motion space that this yielded a list of 1348 stars, illustrated in Figures 5.

To further vet this list, we used NOMAD ( $B - V$ ) and 2MASS ( $J - K_S$ ) color - magnitude diagrams to identify stars consistent with an assumed distance of 230 pc, mid-

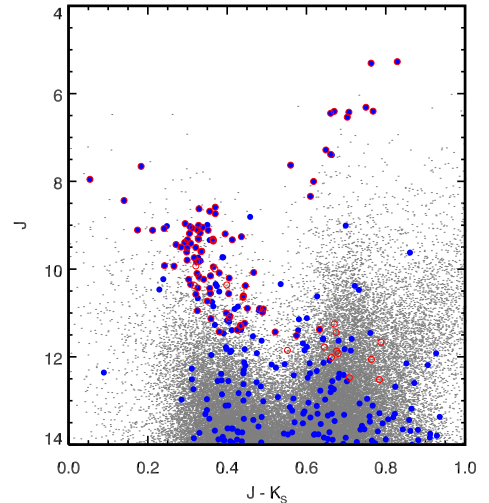


**Figure 5.** Proper motion cuts made to NOMAD stars to identify candidate R147 members. Of the over 750,000 NOMAD stars in the  $1^\circ.5$  radius region centered on R147, 38,623 have  $0 < J - K_S < 1$  and  $4 < J < 14$  which are shown in gray. There are 1348 stars with NOMAD proper motions within 5 mas/yr of the cluster value, which are plotted in blue. Our final membership list of 108 stars are circled in red. This plot demonstrates that there is really only one obvious sequence at bright magnitudes where the proper motions are reliable, including a well-defined red giant branch.

way between the Hipparcos-derived distance to the cluster (250 pc) and the value of Kharchenko et al. (175 pc). We combined the CMDs and proper motion information to estimate crude membership probabilities based on the Hipparcos main sequence with no reddening corrections, calculated generously to account for uncertainties in the cluster parameters and for the poor quality of some of the NOMAD proper motion entries. These membership probabilities also favored brighter targets to improve the efficiency of vetting candidate members at the telescope.

We drew from this list, sorted by membership probability, to choose targets for spectroscopic study at Lick Observatory. We used these spectra to measure radial velocities for the stars and determine the space motion of the cluster.

#### 2.2.1. Data Acquisition and Raw Reduction

We adopted the spectrograph setup procedure of the California and Carnegie Planet Search, which placed bright emission lines from a thorium-argon (ThAr) lamp on specific pixels to approximately reproduce a known wavelength solution to a fraction of a pixel. Our prior experience using the basement-mounted Hamilton spectrograph revealed that the wavelength solution is reliable to a pixel or two over the course of the night. This was sufficient for our purposes of measuring radial velocities to  $< 5 \text{ km s}^{-1}$ , a precision which allows most interloping field stars to be identified, so we did not attempt any further wavelength calibration throughout the night. In practice, our radial velocity accuracy proved to be much better than  $5 \text{ km s}^{-1}$ .

Observing conditions were good, and we obtained several high SNR spectra of radial velocity standard stars of various spectral types throughout the night, chosen from the catalog of Nidever et al. (2002). For candidate

members we used exposure times of 60 – 90 s, depending on the magnitude of the star. For fainter stars we obtained SNRs as low as 1 per pixel, which is sufficient for our velocity work because of the broad spectral coverage of the Hamilton spectrograph. This strategy allowed a large number of stars to be observed in our allocated time for this low-declination cluster, which only spent a few hours per night at sufficiently low airmass to be useful.

The raw spectra were processed with the standard Hamilton Spectrograph data reduction pipeline used for precise radial velocity work by the California and Carnegie Planet Search, which includes bias subtraction and flat fielding of each frame and which results in a one-dimensional spectrum for each of 92 orders.

We calculated an empirical blaze function for each order by fitting a polynomial to the spectra of several rapidly rotating B stars that we observed for this purpose. These stars show no high resolution spectral features, and we corrected orders contaminated by the effects of the broad Balmer lines by averaging the polynomial blaze function of the neighboring orders. Variations in slit illumination from target to target created apparent continuum variations that were not perfectly removed by this process, and the nature of the polynomial fitting process caused the fit to diverge from the actual spectrum significantly at the edges of orders. The resulting spectra were nonetheless sufficiently flat that the cross correlations required for our data analysis (§2.2.3) could be confidently performed.

### 2.2.2. Palomar Spectra

We followed a similar procedure at Palomar Observatory to determine membership probabilities and activity measurements of fainter candidate members. Target stars were drawn from the same sorted list that was compiled for the Lick observing run the previous year, including 25 targets that were chosen for follow-up observations based on qualitative examination of the radial velocity measurements derived from the Lick data, either because the signal-to-noise ratio of the Lick data was too low for a definitive velocity measurement or the star showed evidence of binarity, necessitating a second epoch.

We observed on 2008 August 5 and 18 with the East-Arm Echelle ( $R \sim 33,000$ ; Peri 1995) on the Hale 200-inch at Palomar, following our earlier procedure of short integrations at very low signal-to-noise ratio (the additional aperture of the 200-in over the 3-m, somewhat mitigated by the low throughput of the East Arm Echelle, allowed us to explore fainter targets, or brighter targets at better SNR).

### 2.2.3. Radial Velocity Determination

Although we adopted the rough wavelength calibration used for planet search work, we did not attempt to use this calibration to measure our radial velocities. Rather, we extracted radial velocities in pixel space by cross-correlating the spectra of our candidate cluster members with those of our observed RV standard stars. To reduce the errors introduced by comparing two stars of different spectral types, we paired each candidate member to an RV standard star that minimized the difference between their  $V - J$  colors ( $\Delta(V - J)$ ), with  $V - J = 0.8$  for the bluest standard star and  $V - J = 2.4$  for the reddest.

Imperfect flat fielding produced a sharp spike at exactly zero shift in the cross-correlation functions (CCFs), and the presence of telluric lines created a narrow peak there, complicating the radial velocity measurements derived from these CCFs. This justified our use of velocity standard stars as cross-correlation templates rather than high SNR spectra of actual cluster members, since the standards have different radial velocities than the cluster and so the true CCF peak is far removed from the spurious peak at zero shift. To further address the problem of telluric lines, we empirically rejected those portions of the spectrum where these lines dominated the CCF: after dividing each of the 92 orders into three segments, we discarded from all spectra those segments that showed strong telluric peaks near zero shift.

Computing these CCFs for the different combinations of RV standard stars with  $\Delta(V - J) < 0.5$  allowed us to calibrate the conversion from pixel space shifts to radial velocities, after applying a barycentric radial velocity correction. This calibration step thus obviates the need for a transformation into wavelength space. Specifically, we fit a linear function with zero intercept to the measured RV standard stars' CCF pixel shifts as a function of the difference in their radial velocities, giving us the velocity shift per pixel in each spectrum segment. The root mean squared of the residuals of this fit is less than  $0.6 \text{ km s}^{-1}$ ; this provides our best measure of the systematic velocity precision we expect at high SNRs.

Comparison of this calibration constant among the segments confirmed that the velocity shift per pixel of the Hamilton spectrograph is nearly constant for each of the 92 orders. This is not surprising given that both the resolution,  $R (= \lambda/\Delta\lambda \text{ per resolution element})$ , and the sampling,  $s$  (pixels/resolution element), are nearly constant across an echellogram, and that our calibration constant, having units of  $\text{km s}^{-1}/\text{pixel}$ , is essentially  $c/Rs$ , where  $c$  is the speed of light. This allowed us to add the CCFs of the remaining segments together to improve the SNR of the stellar signal, and enabled the clear identification of a peak and its associated pixel shift in the combined CCF. To be conservative, we divided each spectrum into three sets of segments, corresponding to the left, middle and right sides of each order. After separately summing the CCFs in each set, we required that the location of the tallest peak in the summed CCFs to be identical in all three sets; however, when the side segments produced noisy CCFs, as was the case for stars with  $\text{SNR} \sim 10$ , we used the location of the tallest peak in the middle segments' summed CCF, as long as the peak met our high quality classification.

We visually inspected each CCF produced by our procedure and classified the stars into two categories based on the quality of their CCFs: either the combined CCF had one clear peak, which corresponded to high SNR spectra, or the combined CCF had multiple peaks of approximately equal height, which indicated that the CCF was dominated by noise, and which usually corresponded to spectra with  $\text{SNR} \lesssim 2$  per pixel (some of these discarded stars were later revisited in the Palomar observing run in order to acquire higher SNR spectra).

We found a clear clustering of barycentric velocities near  $43 \text{ km s}^{-1}$ , which is within  $2 \text{ km s}^{-1}$  of the cluster RV quoted by Dias et al. (2002) that was based on a

single measurement of a single putative member (§3.1). Upon closer inspection of the Lick velocities for signs of systematics, we found that these apparent cluster members' velocities exhibited a slight correlation with time from the beginning of the observing run to the end, with magnitude  $2 - 4 \text{ km s}^{-1}$ . We fit this trend to a linear function and removed it. We have also observed 49 of these stars with MMT/Hectochelle (with very high signal-to-noise ratio, we expect all to have RV precision  $\approx 0.5 \text{ km s}^{-1}$ , §2.5), and measure differences between the Lick/Palomar and Hectochelle RVs as large as  $5 \text{ km s}^{-1}$ , except for a possible SB1 with a difference of  $20 \text{ km s}^{-1}$ . We interpret this offset between telescopes and spectrographs as a measure of systematic error in our absolute barycentric radial velocities.

Figure 8 illustrates the resulting RVs and shows a clear clustering around the cluster velocity. We tentatively identified as cluster members any stars with a measured radial velocity between  $32$  and  $54 \text{ km s}^{-1}$ , or roughly twice the typical systematic error.

### 2.3. Optical Photometry

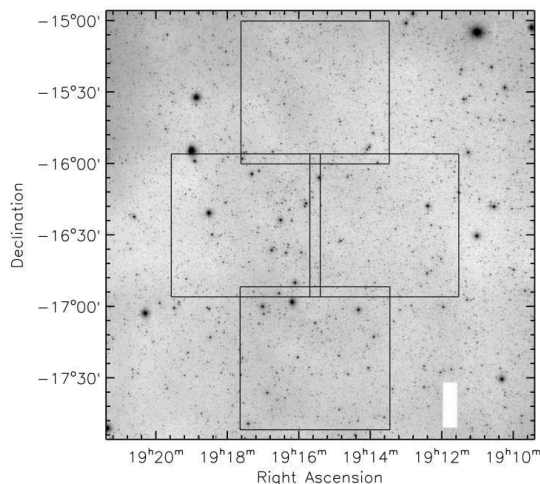


**Figure 6.** The four fields we imaged in  $g'r'i'z'$  with CFHT/MegaCam, overlaid on a 2MASS  $J$  band mosaic image generated with Montage (<http://montage.ipac.caltech.edu>). We log-scaled and smoothed the image with a  $3''$  boxcar.

We imaged a 4 square degree field in the optical  $g'r'i'z'$  bands in 2008 April and May with CFHT/MegaCam (Hora, Luppino, & Hodapp 1994). The observations are summarized in Table 1. With MegaCam's one square degree field of view, four fields were required to cover the majority of the known cluster; the fields are outlined over a 2MASS  $J$  band mosaic image in Figure 6. Six additional surrounding fields were imaged solely in  $i'$  band, for the purpose of first-epoch astrometry for the entire cluster, including any extended halo. We obtained both short and long exposures, providing reliable photometry down to  $g' \sim 25$ , with a bright saturation limit of  $g' \sim 9$ .

TERAPIX kindly provided photometric reduction of

our MegaCam imagery (Bertin et al. 2002)<sup>12</sup>. We merged the short exposure (bright source) and long exposure (faint source) catalogs by matching stars in each catalog, and locating the magnitude where the absolute value of their difference is minimized. The left panel of Figure 7 plots the  $g'$  band photometry from the bright catalog versus the absolute value of the difference between the bright and faint catalogs, along with a natural spline fit illustrating the typical difference for each magnitude. The difference is minimized at  $\sigma'_g = 0.019$  at  $g'_b = 17$ . This minimum value provides an estimate of the photometric precision independent of the errors quoted by TERAPIX (median of  $0.0006 \text{ mag.}$  for R147 stars). Photometry for stars fainter than 17<sup>th</sup> magnitude in  $g'$  is drawn from the faint (long exposure) catalog, and photometry for stars brighter than 17<sup>th</sup> magnitude is drawn from the bright (short exposure) catalog.

We also estimate the photometric error by making use of the overlapping regions between the four imaged fields (see Figure 6). We matched all stars in the overlap regions in our bright source catalog (short exposures), and find a total of 1575 unique sources with  $g' < 18$ . The right panel of Figure 7 plots the mean versus standard deviation of  $g'$  for the  $2 - 4$  independent measurements, depending on the number of overlapping regions containing the source. We find a typical value of  $\sigma_{g'} = 0.035 \text{ mag.}$ , but this is probably larger than what should be assumed for the photometric precision across the field, because one of the sources usually lies very close to the edge of one of the CCD chips, and photometry is unreliable.

The average CCD quantum efficiency over the  $z'$  band filter is only 20%, compared to 85%, 69% and 55% for  $g'$ ,  $r'$  and  $i'$  band. There is strong fringing<sup>13</sup>, so we neglect  $z'$  band in this work, and instead solely analyze the  $(g' - i')$  CMD.

### 2.4. Spectra from Keck/HIRES

Spectra of four cluster members were obtained on 2008 September 12 and 18 and for two members on 2011 October 17 with the High Resolution Echelle Spectrometer (HIRES, Vogt et al. 1994) on the 10-m telescope at Keck Observatory. The stars were kindly observed by the California Planet Survey team (CPS<sup>14</sup>) without an iodine cell, and with the B5 decker (slit of  $3.5''$  length and  $0.861''$  width), giving a typical resolution  $R \sim 50,000$  in the  $3360 - 8100 \text{ \AA}$  bandpass. Exposure times were monitored with a photomultiplier tube exposure meter to ensure high signal-to-noise ( $S/N \sim 50 - 100$ ). These observations are summarized in Table 2, and were reduced by the standard CPS pipeline. Chubak et al. (2012, in prep), measured absolute radial velocities (results discussed in §3.1) and we derive stellar properties in Section 4.2.

### 2.5. Spectra from MMT/Hectochelle

We obtained high-resolution spectra with MMT/Hectochelle in the vicinity of the Ca II H & K

<sup>12</sup> TERAPIX is a data reduction center located at the Institut d'Astrophysique in Paris, France: <http://terapix.iap.fr/>

<sup>13</sup> <http://www.cfht.hawaii.edu/Instruments/Imaging/Megacam/specsinformation.html>

<sup>14</sup> <http://exoplanets.org/cps.html>

**Table 1**  
CFHT/MegaCam observations during Spring 2008: PI John Johnson, observation run ID 2008AH22

Field Name	RA (h:m:s)	Dec (d:m:s)	MegaCam Filter	Exposure Time (seconds)	Number of Exposures
North	19:15:32.65	-15:30:14.20	g	1	5
North	19:15:32.65	-15:29:44.20	r	1	6
North	19:15:32.65	-15:30:14.20	i	1	5
North	19:15:32.65	-15:30:14.20	z	1	5
East	19:17:29.00	-16:26:2.20	g	1	5
East	19:17:29.00	-16:26:2.20	r	1	5
East	19:17:29.00	-16:25:32.20	i	1	13
East	19:17:29.00	-16:26:2.20	z	1	5
West	19:13:36.30	-16:26:2.20	g	1	5
West	19:13:36.30	-16:26:2.20	r	1	5
West	19:13:36.30	-16:26:2.20	i	1	5
West	19:13:36.30	-16:26:2.20	z	1	5
South	19:15:32.65	-17:21:50.20	g	1	5
South	19:15:32.65	-17:21:50.20	r	1	5
South	19:15:32.65	-17:21:50.10	i	1	5
South	19:15:32.65	-17:21:50.20	z	1	5
North	19:15:33.20	-15:30:14.20	g	327	10
North	19:15:32.65	-15:30:14.10	r	163	5
North	19:15:32.65	-15:30:14.30	i	74	5
North	19:15:32.65	-15:30:14.20	z	204	5
East	19:17:29.00	-16:26:2.20	g	327	7
East	19:17:29.00	-16:26:2.20	r	163	5
East	19:17:29.00	-16:26:2.30	i	74	5
East	19:17:29.00	-16:26:2.20	z	204	5
West	19:13:36.30	-16:26:2.20	g	327	5
West	19:13:36.30	-16:25:32.20	r	163	7
West	19:13:36.30	-16:26:2.20	i	74	15
West	19:13:36.30	-16:26:2.10	z	204	5
South	19:15:32.65	-17:21:50.20	g	327	5
South	19:15:32.65	-17:21:50.20	r	163	5
South	19:15:32.65	-17:21:50.20	i	74	5
South	19:15:32.65	-17:21:50.20	z	204	5

**Table 2**  
Keck/HIRES observations.

CWW ID	2MASS ID	Obs Date JD	Exposure Time seconds	Airmass	$V^a$ mag.	S/N <sup>b</sup>	Class <sup>c</sup>
72	19165800-1614277	2008-09-12	210	1.43	11.52	50	SB2
78	19160879-1524279	2008-09-12	170	1.44	11.82	60	late F dwarf
21	19132220-1645096	2008-09-18	90	2.17	9.98	80	Subgiant
22	19172382-1612488	2008-09-18	93	2.12	10.04	70	mid F MSTO / SB1?
44	19164495-1717074	2011-10-17	167	1.39	10.61	80	mid-F dwarf MSTO
91	19164725-1604093	2011-10-17	822	1.32	12.39	50	G0/2 dwarf

<sup>a</sup>  $V$  magnitudes are drawn from the NOMAD catalog.

<sup>b</sup> Signal-to-noise ratio measured in the spectral order encompassing the Mg b triplet, in the 5034 – 5036 Å continuum.

<sup>c</sup> Approximate classification, performed by matching spectroscopic and photometric properties to isochrone masses (§3.2). SB1 status suggested by inconsistent RVs from multiple epochs; MSTO = main sequence turnoff

lines for 48 members (as determined from Lick/Palomar RVs), 10 candidate members (from astrometry and photometry alone), and 23 potential astrometric reference stars. These data provide radial velocities, chromospheric activity indicators (Wright et al. 2004), and gravity diagnostics (via the Wilson-Bappu effect, Wilson & Vainu Bappu 1957) useful for identifying background giants as astrometric references.

MMT is a 6.5-m telescope located at the Fred Lawrence Whipple Observatory on Mt. Hopkins, AZ (Fabricant et al. 2004). Hectochelle is a high-resolution ( $R \sim 32,000 - 40,000$ ) fiber-fed spectrograph, which provides simultaneous observations for 240 targets in

a one square degree field (Szentgyorgyi et al. 1998; Fürész, Szentgyorgyi, & Meibom 2008). We observed the central square degree with the ‘Ca41’ Ca II H & K filter with 1x1 on-chip binning. Eight total hours were obtained to ensure sufficient signal-to-noise for a future chromospheric activity study. All observed targets have  $g' = 9 - 15.5$ .

Twelve 40-minute exposures were obtained over the nights of UT 2010 July 4 – 5. These data were reduced with an IRAF<sup>15</sup>-based automated pipeline developed at

<sup>15</sup> IRAF is distributed by the National Optical Astronomy Observatories, which are operated by the Association of Universities



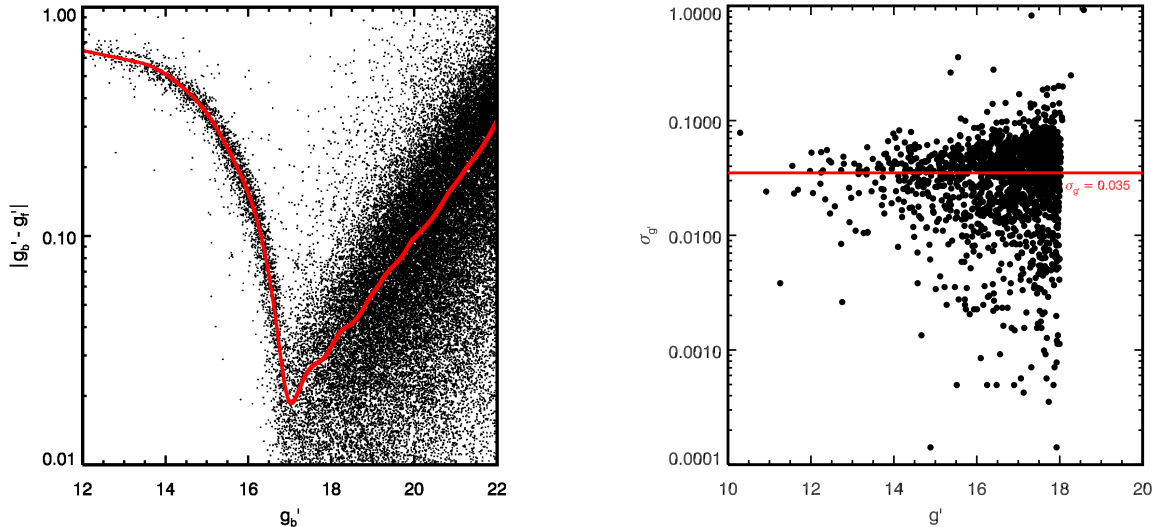


**Figure 7.** Photometric error estimates for CFHT/MegaCam  $g'r'i'z'$  photometry: **Left Panel** – We obtained short and long exposures of the R147 field and merged the corresponding bright and faint source catalogs. The bright source catalog  $g'$  magnitude ( $g'_b$ ) is plotted against the absolute value of the difference for over  $10^5$  stars. The red line plots a natural spline fit, illustrating the typical difference for a given magnitude, with a minimum of  $\sigma_{g'} = 0.019$  at  $g'_b = 17$ . Photometry for stars brighter than  $17^{\text{th}}$  magnitude should be taken from the “bright” catalog, while fainter stars should be taken from the “faint” catalog. **Right Panel** – We imaged the R147 field with four separate but partially overlapping pointings (see Figure 6). We matched all stars in the overlap regions in our bright source catalog (short exposures), and find a total of 1575 unique sources with  $g' < 18$ . This figure plots the mean versus standard deviation of  $g'$  for the 2 – 4 independent measurements, depending on the number of overlapping regions containing the source. We find a typical value of  $\sigma_{g'} = 0.035$ , but this is probably larger than what should be assumed for the photometric precision across the field, because one of the sources usually lies very close to the edge of one of the CCD chips, and is unreliable.

the Harvard-Smithsonian Center for Astrophysics, provided and run by Gabor Fűrész and Andrew Szentgyorgyi, which flat-fielded, cosmic-ray removed, and wavelength calibrated our targets and sky flats. The wavelength solution was determined from Thorium-Argon (ThAr) lamp comparison spectra, with an RMS precision of  $0.2 - 0.5 \text{ km s}^{-1}$  (for reduction details, see Mink et al. 2007).

Radial velocities were measured by cross-correlating the target spectrum with Solar spectra obtained from the sky flat exposures, then corrected for Earth’s heliocentric motion. We checked the fiber-to-fiber and day-to-day stability of the spectrograph by measuring velocity shifts determined by cross-correlating matched ThAr, Solar, and target spectra. The fiber-to-fiber velocity shift on the first night was  $12 \pm 35 \text{ m/s}$  (for the ThAr spectra) and  $200 \pm 200 \text{ m/s}$  (for the Solar spectra). We also measure a night-to-night variation between each fiber of  $31 \pm 41 \text{ m/s}$  (ThAr) and  $200 \pm 180 \text{ m/s}$  (Solar). The RVs measured each day for R147 stars show a mean absolute difference of  $0.23 \text{ km s}^{-1}$ . In summary, fiber-to-fiber and day-to-day offsets and errors are well under or comparable to the precision set by the wavelength solution. The RV distribution for 45 member stars is shown in Figure 8, and is discussed in §3.1.

### 3. IDENTIFYING THE RUPRECHT 147 MEMBERSHIP

We identify stars as R147 members based on their common space motion and placement on a color – magnitude diagram. Our initial membership list is drawn from

the NOMAD and UCAC-3 astrometric catalogs and subjected to radial velocity vetting. We queried NOMAD and UCAC-3 for stars within a radius of  $2^\circ$  of the cluster center. Stars were accepted as candidates if their proper motions (§2.1) were within  $8 \text{ mas/yr}$  of the cluster mean (see Figure 3 for a proper motion vector point diagram). We adopted the values of Kharchenko et al. (2005) for the cluster center and mean proper motion: ( $\alpha$  [h:m:s],  $\delta$  [d:m:s]) = (19:16:40, -16:17:59) and ( $\mu_\alpha$ ,  $\mu_\delta$ ) [mas/yr] = (-0.6, -27.7) – after we identified the highest confidence members, we recalculated these locations and note no significant change (Table 5).

Table 6 gathers data for 108 stars of interest. The first column provides a designation internal to this paper: CWW # (CWW = Curtis, Wolfgang and Wright). The stars are ordered according to increasing  $V$  magnitude (provided by NOMAD). The table also includes the 2MASS ID (and therefore RA and Dec position); proper motions in mas/yr, with a reference flag – NO = NOMAD, U3 = UCAC3, AK = Dr. Adam Kraus (private comm.); CFHT/MegaCam  $g'$  and  $g' - i'$  optical photometry; 2MASS  $J$  and  $J - K_S$  NIR photometry; and radial velocities  $RV_{LP}$  and  $RV_H$  (Lick/Palomar and Hectochelle, respectively). A membership probability is assigned to each of these data, according to criteria discussed below and summarized in Table 3, and is listed in the order: (1) radial distance in proper motion space from the cluster mean, (2)  $RV_{LP}$ , (3)  $RV_H$ , (4) proximity to cluster locus on the 2MASS ( $J - K_S$ ) CMD and (5) CFHT/MegaCam ( $g' - i'$ ) CMD.

The derivation of quantitative membership probabilities is precluded by the large uncertainties in proper motion and our Lick/Palomar velocities, combined with

the intrinsic spread in the R147 main sequence due to an unresolved binary population and the possibility of differential reddening, along with non-negligible photometric error. Instead we designate three confidence levels: ‘Y’ for *yes this is consistent with cluster membership*, ‘P’ for *possible / probable member*, and ‘N’ for *not likely / non-member*. Each membership criterion is independently assessed and assigned a confidence level designation (whenever data are unavailable, a ‘-’ is assigned instead). The following sections address each criterion, and establish the ranges for each level (summarized in Table 3). The results from all fields are then reviewed and an overall membership confidence level is assigned to each star according to the same ‘Y’, ‘P’, ‘N’ scheme.

We find 86 stars of highest confidence, 18 stars with ‘P’ possible member status, and 4 stars with little to no probability of membership - at least as single star members (multiple star systems could show RVs and photometry inconsistent with membership as we have defined it, while still being gravitationally bound members of R147).

### 3.1. The Cluster Radial Velocity

The General Catalogue of Stellar Radial Velocities (Wilson 1953) contains a single entry for a cluster member: HD 180015 (HIP 94635, classified as K0III, CWW 1). Wilson reported  $RV = 41 \text{ km s}^{-1}$ , with quality designation ‘C’, corresponding to a typical uncertainty =  $2.5 \text{ km s}^{-1}$  and maximum uncertainty =  $5 \text{ km s}^{-1}$ . This was the first and only available RV until Pakhomov et al. (2009) observed three other cluster red giants: HD 179691 (CWW 9) at  $46.7 \text{ km s}^{-1}$ , HD 180112 (CWW 10) at  $40.1 \text{ km s}^{-1}$ , and HD 180795 (CWW 7) at  $40.8 \text{ km s}^{-1}$ , with  $S/N > 100$ , and precision estimated at  $0.5 - 0.8 \text{ km s}^{-1}$ . The RV for HD 179691 is  $6 \text{ km s}^{-1}$  larger than the other two stars, too large to be explained by the cluster velocity dispersion, which implies this star is either a SB1 binary or a non-member. We observed these stars at Lick/Palomar and measure  $RV_{LP} = 42.1, 41.4, 42.4 \text{ km s}^{-1}$ , respectively. While our measurements for the second two stars are in basic agreement with Pakhomov et al. (2009), the velocity for HD 179691 now appears consistent with the cluster mean, supporting its membership and corroborating its SB1 status.

Chubak et al. (2012, in prep) have also measured RVs with rms errors  $\sim 50 \text{ m/s}$  for our three single-lined Keck/HIRES spectra from 2008 (Table 4). We list these here in  $\text{km s}^{-1}$ , with our Lick/Palomar velocities in parenthesis for comparison: the first two are 41.02 (40.8) and 40.35 (41.9). The final Keck target has  $RV = 46.63 \text{ km s}^{-1}$ ; while it was not observed at Lick/Palomar, we did follow up with Hectochelle and measure  $RV = 38 \text{ km s}^{-1}$  on both nights, suggesting this to be a SB1.

Selecting the four stars above showing no evidence of binarity, we find a typical cluster radial velocity of  $40.57 \pm 0.42 \text{ km s}^{-1}$ . We take stars with RVs consistent with this value as high-probability cluster members. Figure 8 plots 98 stars with Lick/Palomar velocities (shown in gray hash) with  $RV_{LP} = 43.8 \pm 3.2 \text{ km s}^{-1}$ . Also shown are 45 stars with Hectochelle velocities (black line) with  $RV_H = 41.6 \pm 1.5 \text{ km s}^{-1}$ . The blue tick mark at

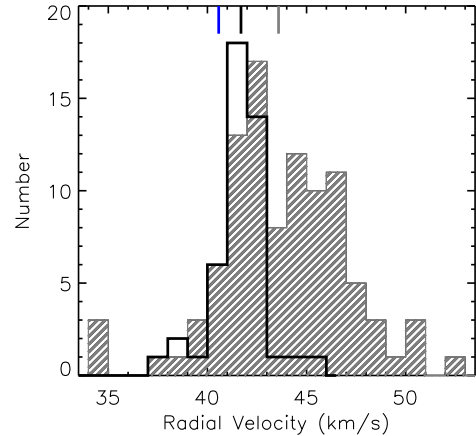


**Figure 8.** R147 radial velocity distribution. The gray hash designates RVs measured from Lick/Palomar (98 stars), with  $RV_{LP} = 44 \pm 3 \text{ km s}^{-1}$ . The black line plots 45 stars with Hectochelle velocities,  $RV_H = 41.6 \pm 1.5 \text{ km s}^{-1}$ . Tick marks on top indicate mean values, color-coded to RV source: blue shows the cluster  $RV = 40.57 \text{ km s}^{-1}$  (described in §3.1). The width of each distribution is as expected from the RV precision of each survey, and should not be interpreted as a resolved cluster velocity dispersion, which should be  $\sigma_v \lesssim 0.3 \text{ km s}^{-1}$ .

the top shows the typical cluster velocity from above at  $40.57 \text{ km s}^{-1}$ . The width of each distribution is consistent with the RV precision of each survey, and should not be interpreted as a resolved cluster velocity dispersion<sup>16</sup>

We have RVs from Lick/Palomar ( $RV_{LP}$ ) for nearly all stars listed in Table 6, except the 6 putative blue stragglers and 4 SB2s; and RVs from Hectochelle ( $RV_H$ ) for 50 stars in the central square degree. The Hectochelle velocities are more precise (Figure 8), so whenever available,  $RV_H$  is used to determine the confidence in membership. Some stars have  $RV_{LP}$  within the highest confidence interval, and  $RV_H$  in a lower level. In these cases, if the star has ‘Y’ confidence level proper motions,  $RV_{LP}$  and photometry, we set the overall confidence to ‘P’, and consider the star a candidate SB1 (e.g. CWW 92 has  $RV_{LP} = 45 \text{ km s}^{-1}$  and  $RV_H = 25 \text{ km s}^{-1}$ ).

### 3.2. The Color - Magnitude Diagram and Stellar Populations

Before assigning membership confidence designations, we check that the stars are confined to the region of color - magnitude space expected for a coeval stellar population with the properties we determine best describe R147.

We mapped out this locus by simulating a rich cluster with the properties we find for R147 from isochrone fitting (§4.4). Figure 9 shows CMDs for such simulated clusters. In this case, we simulated a cluster with  $10^6$  stars, with masses uniformly distributed between  $0.6$  and  $1.6 M_{\odot}$ . We set the binary fraction to 50%, with compan-

<sup>16</sup> M67, a much richer cluster, has a measured velocity dispersion of  $0.5 \text{ km s}^{-1}$  from radial velocities measured by Mathieu (1983). Assuming virial equilibrium, the cluster velocity dispersion can be approximated as  $\sigma_v(\text{kms}^{-1}) \sim \sqrt{\frac{GM}{R}}$ . With  $\sim 500$  known members and similar size, we expect the M67 velocity dispersion to be about twice that of R147.

ion masses uniformly distributed between zero and the primary mass. Differential extinction is introduced according to a Gaussian with  $\mu = 0.25$  and  $\sigma = 0.05$  mag., and photometric precision is set at 0.02 mag. for  $g'r'i'z'$  and 0.025 mag. for  $JHK_S$ . The simulated photometry is drawn from a Padova isochrone with  $\log t = 9.4$  (2.5 Gyr),  $[M/H] = +0.08$ , and  $m - M = 7.35$  mag. We bin, log-scale, and smooth the photometry to highlight the R147 locus in color – magnitude space.

Stars overlying the shaded region (basically, the region bound by the single star and equal mass binary sequences) are given the highest confidence designation. The simulation demonstrates that atypical differential reddening along a particular line of sight or relatively high photometric error can place stars outside the locus. Stars in these regions are assigned ‘P’. These could also be triple systems or exotic products of stellar mergers. CWW 67 is the only star existing beyond the equal mass triple sequence, and we assign it the lowest designation, ‘N’.

Confidence assignment is an iterative process, since we identify high-confidence members using isochrone fits, and these fits require a list of high-confidence members so that unlikely or non-members do not throw off the fit.

### 3.2.1. Stellar Populations

**Blue Stragglers:** In addition to the potential triple systems, 5 – 6 stars occupy a space of the CMD outside the cluster locus beyond the main sequence turnoff (MSTO): 6 clearly separate in the 2MASS CMD, but only 5 in  $g'r'i'z'$ . These five stars have proper motions consistent with the cluster, but lack RV measurements due to rotational line broadening (CWW 24, the sixth outlier in 2MASS, does have a measured  $RV_{LP} = 41.8$  km s<sup>-1</sup>, and so we assume that 2MASS photometric error is responsible for scattering it out of the cluster locus). We classify these stars as blue stragglers (see Table 6, blue stragglers are listed as ‘BS’ in the Notes column).

**Red Giants:** We find 11 red giants in the cluster, 2 of which lack  $g'r'i'z'$  photometry (being outside the CFHT/MegaCam field). The four brightest red giants saturated in  $g'r'i'z'$  even with 1 second exposures. CWW 14 is fainter and has reliable photometry, although it is 0.15 mag. blueward of the red giant branch in  $(g' - i')$ , and 0.08 mag. (4- $\sigma$ ) blueward in  $(J - K_S)$ . Mathieu, Latham, & Griffin (1990) identify a SB1 system in M67, S1040, which lies 0.2 mag. to the blue of the red giant branch in  $(B - V)$ . This system was previously suggested to consist of a star further down the giant branch with a companion star near the MSTO. Landsman et al. (1997) identified broad Lyman absorption features, demonstrating that the companion is actually a hot white dwarf, and that the system likely underwent a period of mass transfer. CWW 14 may be an analogous “red straggler” or MSTO – RGB binary.

**Main Sequence dwarfs:** We use our best isochrone fit to determine approximate spectral types for the R147 membership. We assume masses of 1.1  $M_\odot$  for G0 and 0.8  $M_\odot$  for K0 dwarfs (Zombeck 2007), then locate the boundaries in the CMD from the isochrone. We find that the MSTO is located around mid-F. The subgiant branch down to F8 on the main sequence is well populated with  $\approx 52$  stars. We also identify  $\approx 27$  G dwarfs and  $\approx 8$  K dwarfs down to mid-K (We quote approximate numbers

because of the approximate nature of our spectral typing). The 9 stars lacking  $g'r'i'z'$  photometry appear in the 2MASS CMD as follows: 2 red giants, 3 MSTO F stars, 2 G dwarfs and 2 K dwarfs.

This method ignores the existence of binaries but illustrates the top-heavy nature of our membership list. This is likely due to a combination of observational bias and cluster evaporation (star clusters tend to lose their lowest mass members first, and ‘evaporate’ from the bottom up). The typical NOMAD proper motion error is  $\sim 10$  mas/yr by  $V \sim 12$ . The K dwarfs have  $V > 13$ , making candidate identification from proper motions difficult. Therefore we are almost certainly missing significant numbers of low mass dwarfs.

## 3.3. Notes on Particular Stars

### 3.3.1. Apparent Non-members

We have assigned 4 stars on our list as ‘N’, not likely / non-members.

CWW 77 has RVs inconsistent with R147 ( $RV_{LP} = 51$  km s<sup>-1</sup>,  $RV_H = 52$  km s<sup>-1</sup>), but its  $(g' - i')$  and  $(J - K_S)$  photometry place it near the equal mass binary sequence, so it could be an SB1.

CWW 67 has a low  $RV_{LP} = 34$  km s<sup>-1</sup> and is 1.3 mag. above the  $(g' - i')$  main sequence and 1.4 mag. above in  $(J - K_S)$ , but an equal mass triple would sit 1.2 mag. above the main sequence, so membership seems very unlikely (although a fourth lower mass companion could theoretically explain these discrepancies, so membership is difficult to definitively rule out).

CWW 72 sits  $\approx 1$  mag. above the main sequence in  $(g' - i')$  and  $\approx 0.75$  mag. in  $(J - K_S)$  – if a member, this could be a triple or an equal mass binary with inaccurate optical photometry. CWW 72 is a SB2, as seen in the Keck/HIRES spectrum. This star was observed previously at Lick and the spectrum exhibited no sign of binarity (otherwise we would not have selected it for observation with Keck). We also observed CWW 72 on two consecutive nights with MMT/Hectochelle. The CCF from the first night exhibits a tall and sharp peak with  $RV_{H1} = 46.6$  km s<sup>-1</sup>. The CCF from the second night is lopsided, suggesting that the signature of the companion was beginning to manifest and that the period of this system could be on the order of days. The CCF shape and resulting radial velocity from the first night point to a systematic velocity  $\approx 5$  km s<sup>-1</sup> greater than the R147 bulk motion, which cannot be explained by the cluster’s velocity dispersion or RV precision. If CWW 72 is a member, then it is (at least) a triple, perhaps with two approximately equal mass primary components orbiting with a period of days, and a fainter companion modulating the RV on a longer timescale (needed to explain the 5 km s<sup>-1</sup> systematic offset).

CWW 104 has  $RV_{LP} = 52$  km s<sup>-1</sup> and a proper motion, derived and provided by Dr. Adam Kraus, that is kinematically distinct from R147, though a precise proper motion is difficult to determine as this is the 4<sup>th</sup> faintest star included in this list (proper motions from UCAC-2:  $\mu_\alpha = 0.9$ ,  $\mu_\delta = -18.6$ ; from UCAC-3:  $\mu_\alpha = 16.6$ ,  $\mu_\delta = -4.3$ ; from Adam Kraus:  $\mu_\alpha = 9.1$ ,  $\mu_\delta = -8.6$ ). CWW 104 was originally considered for membership because it is 9 mas/yr from the R147 motion according to UCAC-2).

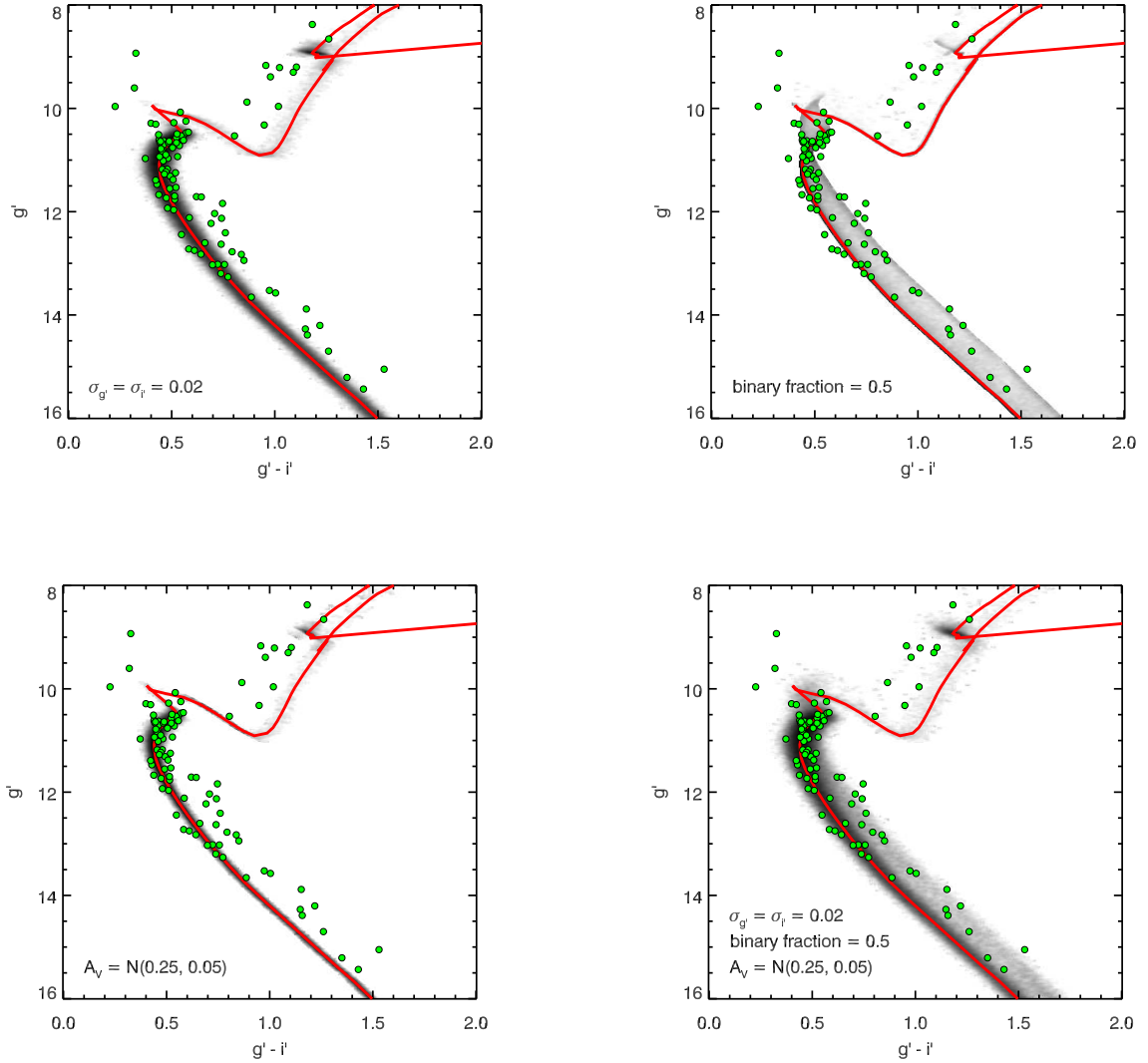


**Figure 9.** Each panel illustrates a source of main sequence broadening, demonstrating why the R147 main sequence might appear thicker than a textbook “beads on a wire” CMD. The R147 stars are plotted in green, along with a Padova isochrone in red with age = 2.5 Gyr,  $m - M = 7.35$  ( $d = 295$  pc),  $A_V = 0.25$ , and  $[M/H] = +0.08$ . The shaded regions in each panel represent simulations of  $10^6$  stars, with masses uniformly distributed between 0.06 and  $1.6 M_{\odot}$ , and photometry queried from the previously quoted Padova model. The simulated photometry has been binned (0.005 mag. in  $g' - i'$ , 0.01 mag. in  $g'$ ), log scaled, and smoothed with a 5 pixel boxcar, to highlight possible regions of color-magnitude space occupied by R147 members. The top-left panel only includes photometric error, set at  $\sigma_{g'i'} = 0.02$  and assuming normally distributed errors. The top-right panel only includes binaries, with the binary fraction set at 50%, and the secondary masses uniformly distributed between zero and the primary mass. The bottom-left panel only includes differential extinction, normally distributed about the typical cluster value of  $A_V = 0.25$ , with  $\delta A_V = N(0, 0.05)$ .

Finally, CWW 50 sits 0.05 mag. blueward of the ( $g' - i'$ ) main sequence, but is on the ( $J - K_S$ ) main sequence. In Section 4.1 we discuss the possibility that this star is less extinguished and reddened than the rest of the cluster. If this is not the case, perhaps a hot white dwarf is pulling it blueward while not introducing much NIR flux, or there is an atypically large photometric error in one of the optical bands ( $2\sigma$ ), or else CWW 50 is not a member. We list it as ‘P’ because it is only inconsistent in ( $g' - i'$ ), and while  $RV_{LP} = 47.6 \text{ km s}^{-1}$ , the Lick/Palomar velocity precision does not rule out membership.

### 3.3.2. Notes on 2MASS photometry

Our  $g'r'i'z'$  imaging shows CWW 51 is an optical double, with a star 1.65 arcseconds away with a similar  $g'r'i'z'$  SED (the magnitude difference in each band is 0.02 – 0.05 mag. between the two stars). This optical double was not resolved in the 2MASS Point Source Catalog. Adding 0.75 mag. to the  $J$  band magnitude (halving the brightness, to reflect just the one star) moves CWW 51 next to the stars it neighbors in the ( $g' - i'$ ) CMD. Table 6 quotes, and the figures in this work plot, the 2MASS photometry for CWW 51, despite this realization, although we do include a footnote referencing this in the Table.

**Table 3**  
Criteria for membership

Data	Source	Highest: Y	Probable: P	Low or Non-member: N
$r_\mu^a$	NOMAD, UCAC-3, Adam Kraus	< 5	5 – 8	> 8
Radial Velocity <sup>b</sup>	Lick & Palomar	39 – 47	36 – 39, 47 – 50	33 – 36, 50 – 53
Radial Velocity ( $J - K_S$ ) CMD	Hectochelle 2MASS	40 – 43 Overlaps with simulation <sup>c</sup>	38.5 – 40, 43 – 44.5 $\pm 0.2$ mag.	else beyond equal mass triples
( $g' - i'$ ) CMD	CFHT/MegaCam	Overlaps with simulation	$\pm 0.2$ mag.	beyond equal mass triples

**Note.** — See Section 4 for a discussion of membership criteria. Values in parenthesis denote acceptable ranges. Values equal to endpoints are assigned to the higher level

<sup>a</sup> Radial distance in proper motion space from the mean value for R147, with units of mas/yr.

<sup>b</sup> Radial velocities measured in km s<sup>-1</sup>.

<sup>c</sup> See Section 3.2 and/or Figure 9 for discussion

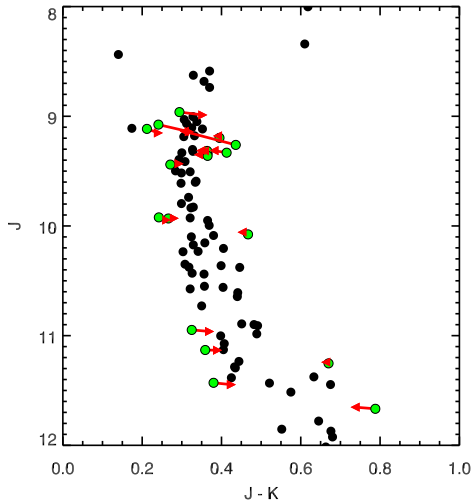


**Figure 10.** PSF photometry (green circles) vs aperture photometry (red triangles) for 18 outliers on the 2MASS ( $J - K_S$ ) CMD. All shift closer to the locus when the aperture photometry is used instead of the default PSF photometry. Only 4 stars already in the locus shift outside when aperture photometry is used instead (not shown).

The 2MASS Point Source Catalog provides PSF photometry by default in most cases. Figure 10 shows 23 outlier stars on either side of the ( $J - K_S$ ) main sequence, out of the 80 stars ‘Y/P’ stars with aperture photometry that are not blue stragglers. If aperture photometry is used instead, each of these stars moves towards the cluster locus, while 4 stars move out of the locus (CWW 10, 21, 40, and 84). We find no resolved doubles in our optical imaging within 5'' for these stars, which would necessitate PSF fitting. The fact that the majority of outliers’ photometry systematically moves toward the cluster locus suggests to us that for many stars in these fields and at these magnitudes, the aperture photometry is superior. We do not assign lower confidence levels to PSF photometry outliers, if their aperture photometry is consistent with membership. We include the aperture photometry for 18 stars in Table 6 and all other figures (CWW 22, 24, 27, 28, 30, 37, 38, 43, 48, 49, 57, 59, 67, 68, 90, 91, 94, and 100).

### 3.3.3. SB2 systems

CWW 64, 65, 66, 68, and 72 showed double-peaked cross-correlation functions in one of the RV epochs, indicating these systems to be nearly equal mass binaries (the case of CWW 72 is discussed above). Figure 11 plots the ( $g' - i'$ ) and ( $J - K_S$ ) CMDs, with the five SB2s highlighted red. The single star and equal mass binary sequences from our best isochrone fit (Padova model) are plotted in green. All five SB2s are clustered around the equal mass binary sequence, corroborating their equal mass status and the validity of our isochrone fit.<sup>17</sup>

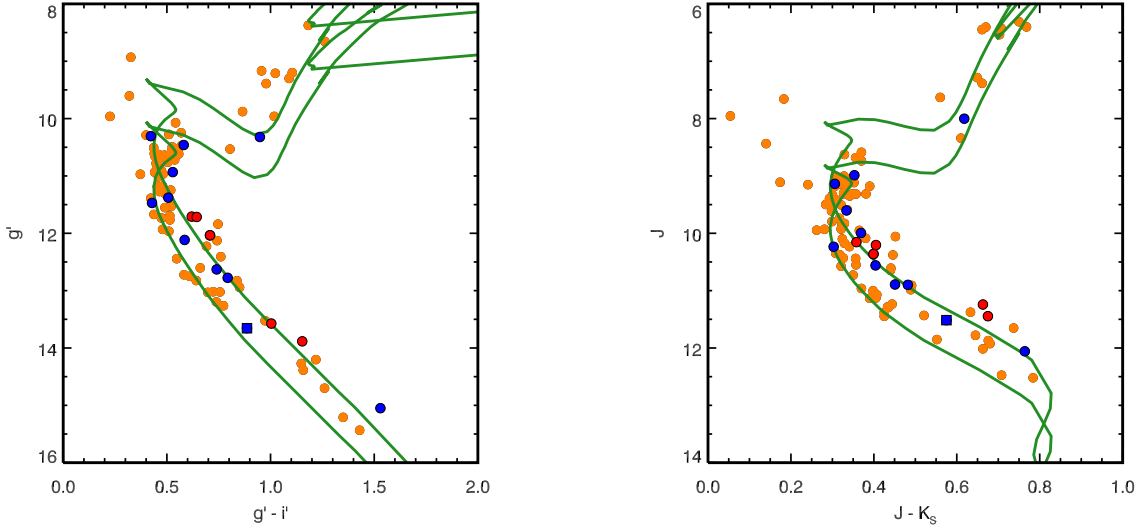
### 3.3.4. SB1 binary candidates from discrepant RVs

Figure 11 also plots in blue 11 stars with Hectochelle RVs inconsistent with the cluster: CWW 19, 22, 27, 53, 69, 70, 77, 92, 95, 99, and 106. In Section 3.1 we suggested CWW 92 is a SB1 from the 20 km s<sup>-1</sup> difference between RV epochs. All other SB1 candidates have similar RVs from Lick/Palomar and Hectochelle, and are considered candidate SB1s because  $RV_H$  is at least a few standard deviations away from the cluster average, although this discrepancy forces a ‘P’ classification (except CWW 77, which we classify as ‘N’ as noted above).

Figure 11 shows all but CWW 70 are clustered around the binary sequence. CWW 70 has  $RV_{LP} = 38$  km s<sup>-1</sup> and  $RV_H = 39$  km s<sup>-1</sup>. Despite this 2- $\sigma$  discrepancy, we cannot rule out membership. The star might have a low mass companion or received a gravitational ‘kick’. For example, a G2 V (1  $M_\odot$ ) – M0 V (0.5  $M_\odot$ ) binary system with semi-amplitude velocity  $K_1 = 5$  km s<sup>-1</sup>, zero eccentricity and zero inclination, will have a period  $P \approx 12$  years. The large luminosity difference in a high mass ratio binary means the system will not stand out in either photometry (it will lie on the single star sequence) or in spectra (the secondary is too faint to manifest as a SB2). This means although the RVs for CWW 70 are inconsistent with single star membership, we cannot rule out the possibility of a low mass companion at large separation, which would induce a measureable velocity offset, but modulated at a period much longer than our 2 year baseline.

CWW 99 is plotted as a blue square in Figure 11. It sits on the single star ( $g' - i'$ ) sequence, but is 0.5 mag.

<sup>17</sup> CWW 68 actually sits on the equal mass triple sequence. Both CWW 64 and 65 are midway between the equal mass binary (-0.75 mag.) and triple (-1.2 mag.) sequences, at 1.0 mag. brighter than the main sequence, which can occur when an equal mass binary system, which manifests as the SB2, has a third companion with 50% the luminosity of each primary.



**Figure 11.** Eleven stars with discrepant Hectochelle RVs are plotted in blue ( $RV_H - 41.5 \pm 1.5 \text{ km s}^{-1}$ ). Five SB2s are plotted in red. The rest of the cluster is shown in orange, with our best fit isochrone (Padova model) overplotted in green showing the single and binary sequences ( $\log t = 9.4$ ,  $[M/H] = +0.1$ ,  $m - M = 7.48$ ,  $A_V = 0.23$ ). All of the SB2s were identified by a double-peaked cross-correlation function, which indicates these should be nearly equal mass ratio systems. The fact that they are all clustered around the binary sequence (shifted “up” 0.75 mag.) corroborates their equal mass status and the validity of our isochrone fit. All but 3 SB1 candidates are also shown near or on the binary sequence. The square shows CWW 99 on the  $(g' - i')$  single star sequence, but in  $(J - K_S)$  the star is 0.5 mag above this sequence. The other two stars might be high-mass ratio systems (and so do not manifest in shifts on the CMD), stars that have received gravitational kicks (so their RVs are no longer consistent with the cluster), or are non-members.

above the  $(J - K_S)$  sequence. This can be explained by a low mass companion, which would show up more prominently in NIR than optical.

#### 4. INFERRING CLUSTER PROPERTIES

The properties of stellar clusters (age, composition, distance and interstellar extinction) are commonly estimated by fitting isochrones to broadband photometric color – magnitude diagrams (CMD). Often a “chibi-eye” technique is employed, where sets of isochrones representing varying cluster parameters are overlaid on a CMD, and the apparent best fit or series of best fits are selected to establish acceptable ranges for these fundamental parameters. This technique can be successful when one or more of these properties can be well constrained. For example, clusters might be nearby or sit above/below the galactic plane and suffer little extinction, and the closest benchmarks have parallax distances from Hipparcos and/or HST/FGS. These independent constraints break the high degree of degeneracy between each variable (e.g. metallicity works in a similar direction to the interstellar reddening vector).

None of Ruprecht 147’s properties have been previously well measured. At a distance of over 200 pc, the cluster has a HIP2 distance measurement from 2 stars that appears unreliable and is apparently too close by a significant fraction. We first describe our efforts to independently constrain the interstellar extinction with the Schlegel, Finkbeiner, & Davis (1998) dust map (§4.1), and the composition from spectroscopic analysis (§4.2), then we will use isochrone models to determine the cluster’s age and distance. Specifically, we fit a spectroscopically derived  $T_{\text{eff}} - \log g$  diagram with Padova isochrones with abundances fixed by the spectroscopic metallicity (§4.3). We then query the resulting best fit Padova

isochrone for a star with  $T_{\text{eff}}$  and  $\log g$  closest to the values for the G0/2 dwarf we derive with SME, and perform a brute force  $\chi^2$  SED fit for distance and visual extinction to the resulting synthetic  $g'r'i'JHK_S$  photometry. Next we fit the  $(g' - i')$  and  $(J - K_S)$  CMDs with isochrones to determine the distance and visual extinction, with the spectroscopic age providing the constraint necessary to break the high degree of degeneracy between these parameters (§4.4). We will see that in the optical, the resulting best fit isochrone well matches the main sequence turnoff and FG dwarf sequence, but fails to accurately describe the K dwarfs and red giants, although the model does represent all CMD features in the NIR (Figures 18, 19). In Section 4.4.1, we search a range of ages and metallicities for an alternative solution, using a 2D cross-correlation isochrone fitting technique and find that the overall optical CMD appears to be best fit by a much older model, but this model fails in the NIR and is inconsistent with our spectroscopic results. Finally, we synthesize the results from these various isochrone fits and present our preferred set of parameters describing the age, composition, distance and visual extinction for Ruprecht 147 (§4.4.2), and suggest that the discrepancy between our preferred model and the optical CMD is possibly due to model deficiencies resulting from line blanketing in the optical in the atmospheres of cooler, super-Solar metallicity stars.

##### 4.1. Interstellar Extinction

The large apparent size of R147 on the sky introduces the possibility of differential extinction across the cluster. Figure 12 plots  $A_V$  from the dust map of Schlegel, Finkbeiner, & Davis (1998), assuming  $R_V = 3.1$ , with R147 members overlaid. Many cloud structures are apparent in the field, showing  $A_V$  to vary from

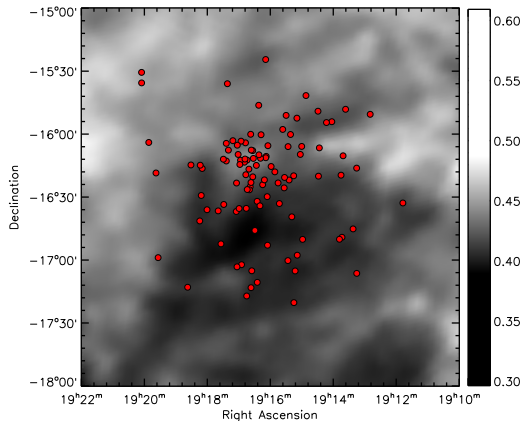


**Figure 12.** Visual extinction map with R147 members designated by red dots.  $A_V$  calculated from the dust map of Schlegel, Finkbeiner, & Davis (1998), assuming  $R_V = 3.1$ . The map was smoothed with a 3 arcminute boxcar.

0.3 – 0.5 mag.

Considering the cluster’s proximity, some of this dust undoubtedly lies beyond the cluster. Drimmel & Spergel (2001) determine the Sun to lie  $14.6 \pm 2.3$  pc above the Galactic midplane, and measure a dust scale height of  $h_d = 188$  pc at the Solar Circle. The Galactic latitude of R147 ranges from  $-12^\circ$  to  $-14^\circ$ . At a distance of 250 – 300 pc, this latitude places R147 50 – 70 pc below the Sun, and 35 – 55 pc below the midplane (less, if a larger  $Z_\odot$  is assumed), or about 20-30% of the dust scale height. The local bubble has very little dust in it out to  $\sim 150$  pc (Lallement et al. 2003), suggesting it is possible that most of the dust is behind the cluster.

Section 3.2 described star cluster simulations used to assess photometric membership probabilities, by introducing photometric scattering sources to explain the observed width of the R147 main sequence, including photometric error, binarity, and differential extinction. Figure 9 plots simulated cluster CMDs including each of these photometric scattering sources separately, and all combined. The binarity simulation demonstrates that the single star and equal mass binary sequences pinch together near the MSTO. Differential reddening smears the CMD along a negative-sloped diagonal (extinction plus reddening). If there is non-negligible differential reddening, the “binary pinch” should be smeared out.

Unfortunately, we have only identified 6 members at this pinch. Figure 13 shows four are confined within the pinch. CWW 50 sits 0.08 mag. blueward, and CWW 53 sits 0.06 mag. redward. These values are 2 – 3 times larger than the expected photometric error. CWW 53 has RVs from two epochs at  $5 \text{ km s}^{-1}$  greater than the cluster mean, and photometry placing it near the equal mass triple sequence. The uncertainty in membership and multiplicity means we cannot use CWW 53 to test for differential reddening. CWW 50 must be reddened by  $\delta A_V = 0.13$  mag. in order to place it on the single star sequence. In Section 4.3, we find an optimal  $A_V = 0.23$  mag., so a particular line of sight of  $A_V = 0.10$  mag. is not impossible. Ideally, we would like to check if the nearest R147 neighbors to CWW 50 also appear less extinguished than expected. Unfortunately, the near-

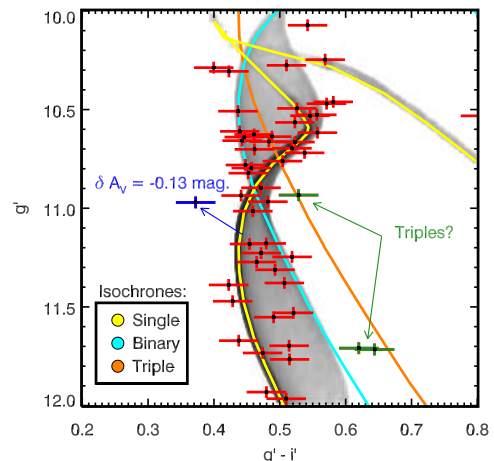


**Figure 13.** Looking for differential extinction. The ‘Y’ and ‘P’ members are plotted with 0.03 mag. error bars in color and magnitude. Single star and equal mass binary sequence isochrones (Padova) are plotted with  $\log t = 9.4$ ,  $[M/H] = +0.1$ ,  $m - M = 7.48$ , and  $A_V = 0.23$ . The single and binary sequences form a “pinch” at the turnoff. Differential extinction should smear this pinch along the reddening vector shown in blue. The three outliers redward of the binary sequence could be triples. CWW 50, the one outlier blueward of the single star main sequence, might either suffer atypically large photometric error, or is not a member, or else needs to be de-reddened by  $\delta A_V = 0.13$  in order to place it on the main sequence. Interestingly, the visual extinction from the Schlegel, Finkbeiner, & Davis (1998) dust map at the position of CWW 50 is the lowest in the field, and exactly 0.13 mag. lower than the median value for the region of radius  $r = 1''.2$  centered on the cluster and encompassing all R147 members.

est neighbor is  $\sim 10'$  away. It is also noteworthy that the Schlegel, Finkbeiner, & Davis (1998) dust map extinction along this line of sight is  $A_V = 0.296$  mag., the lowest value in the entire field, and 0.13 mag. lower than the median  $A_V$  for the region of radius  $r = 1''.2$  encompassing all R147 members.

The R147 main sequence is thicker than 1 magnitude at various points. Unfortunately in many cases, our radial velocities do not have sufficient precision to firmly establish these stars as cluster members (we still designate them ‘Y’ members because the RVs are consistent with the R147 bulk motion, within the precision of our Lick/Palomar RV survey). We also only have one RV epoch for the majority of stars, and so stellar multiplicity is impossible to diagnose at this point. More precise velocities are required before we attribute these photometric outliers to differential extinction.

There is also a strip of 7 main sequence dwarf stars blueward of our best isochrone fit. Adding  $\delta A_V = 0.05$  mag. to these stars shifts them onto the isochrone. This translates into a 0.03 mag. shift in color, which is within the photometric precision, and so differential extinction is not required to explain these stars apparent blueward offset in the optical CMD. No net offset is seen in the NIR CMD.

We will postpone our investigation into differential extinction to a future study, and in this work will fit single  $A_V$  models, with values constrained by the dust map at  $A_V < 0.5$ .

#### 4.2. Metallicity

We analyzed five Keck/HIRES spectra with Spectroscopy Made Easy (SME, Valenti & Piskunov 1996), using the procedure described in Valenti & Fischer (2005). SME uses the Levenberg-Marquardt algorithm to fit observed echelle spectra with synthetic spectra generated assuming LTE and plane-parallel geometry, yielding effective temperature, surface gravity, metallicity, projected rotational velocity, and abundances of the elements Na, Si, Ti, Fe, and Ni<sup>18</sup>

Upon obtaining an initial fit to a spectrum,  $T_{\text{eff}}$  was perturbed  $\pm 100\text{K}$  and run again. The three solutions were then averaged, with the standard deviation set as the parameter uncertainty, except in cases where this uncertainty is less than the statistical uncertainties measured in Valenti & Fischer (2005): 44 K in effective temperature, 0.03 dex in metallicity, 0.06 dex in the logarithm of gravity, and  $0.5 \text{ km s}^{-1}$  in projected rotational velocity. Additional corrections are applied to the final values based on the analysis in Valenti & Fischer (2005) of Vesta and abundance trends in binary pairs with  $T_{\text{eff}}$  (see Figure 14 for the CWW 44 Keck/HIRES spectrum and SME synthetic spectrum fit in the order encompassing Mg b).

Our initial results for the five stars are presented in Table 4 and indicate that the cluster has a slightly super-Solar metallicity of  $[\text{M}/\text{H}] = +0.08 \pm 0.03$ . We neglected the results from CWW 22 because it is hottest (complicating the fit to gravity, described in the next subsection) and has the poorest  $\chi^2_{\nu}$  fit. Valenti & Fischer (2005) suggest using  $[\text{Si}/\text{H}]$  as a proxy for the  $\alpha$ -process abundance. We find  $[\alpha/\text{Fe}] = [\text{Si}/\text{H}] - [\text{Fe}/\text{H}] \approx 0.0$  ( $[\text{Si}/\text{Fe}] = -0.03$  and  $0.0$  for CWW 44 and 91).

We find a much lower metallicity for CWW 78,  $[\text{M}/\text{H}] = -0.11 \pm 0.03$  and  $[\text{Fe}/\text{H}] = 0.0 \pm 0.02$ . This outlier has otherwise satisfied every criterion for membership, with proper motions, photometry and a precise RV all consistent with the cluster. For this work, we will assume that this peculiar metallicity can be explained by a complication in the SME analysis, or binarity (CWW 78 sits 0.3 mag. above or 0.05 mag. redward of the  $(g' - i')$  main sequence, but is not offset from  $(J - K_S)$  CMD. This could be explained by a single star with measurement error in one of the optical bands, or a binary with error in the NIR that shifts it onto the single star sequence).

Pakhomov et al. (2009) analyzed high-resolution, high signal-to-noise spectra of three red giant members of R147, and their results are compiled in Table 4. The first star, HD 179691, has a radial velocity inconsistent with the cluster, indicating it is either an SB1 or not a member. The other two red giants show super-Solar iron abundance, consistent with our SME results.

In the future, we will more rigorously determine the cluster metallicity combining photometry, spectroscopy,

<sup>18</sup> Valenti & Fischer (2005) did not solve for magnesium abundance because of the degeneracy between  $[\text{Mg}/\text{Fe}]$  and  $\log g$  when fitting the synthetic spectra to the gravity-sensitive Mg b triplet (Thackeray 1939). Fuhrmann et al. (1997) recommends fitting for  $[\text{Mg}/\text{Fe}]$  first, using the weak Mg i lines at  $\lambda 4571$  or  $\lambda 5711$ , and then fixing the abundance and fitting the Mg b wings to derive  $\log g$ . Valenti & Fischer (2005) decided to exclude from analysis wavelengths  $\lambda < 6000 \text{ \AA}$ , except for the region encompassing the Mg b triplet, because of severe line blending in the blue in cool stars which would complicate the spectral synthesis fit.

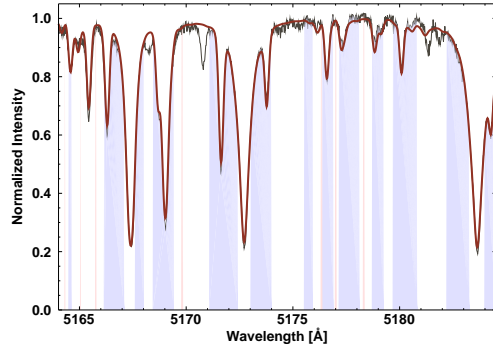


**Figure 14.** A Keck/HIRES spectrum of the order encompassing the Mg b triplet for CWW 44, an F MSTO star, is shown in black. The synthetic spectrum resulting from our SME analysis is overlaid in red. The spectrum segments included in the fit are highlighted in purple, and the salmon stripes identify the continuum regions. Table 4 lists our SME results for this and four other stars.

and cluster properties.

#### 4.3. Fitting Isochrone Models to Spectroscopic Properties

Figure 15 shows the  $T_{\text{eff}} - \log g$  diagram resulting from our SME analysis, along with a  $(g' - i')$  CMD for the 5 stars, along with their CWW IDs. The CMD shows that our SME results place the stars on the  $T_{\text{eff}} - \log g$  diagram with the correct relative positions. We have selected Padova isochrone models with  $[\alpha/\text{Fe}] = 0$  and  $[\text{M}/\text{H}] = +0.1$ , and attempt a “chi-by-eye” fit by overlaying models with ages at  $\sim 2, 2.5,$  and  $3 \text{ Gyr}$  ( $\log t = 9.3, 9.4, 9.5$ ). Fitting the  $T_{\text{eff}} - \log g$  diagram is powerful because it is independent of  $m - M, A_V,$  and color - temperature transformations.

The MSTO star CWW 44 in theory provides a tight constraint on age and metallicity, but we are cautious of the accuracy of  $\log g$ , because the broad wings of the Mg b lines provide the gravity constraint, and their sensitivity decreases at higher temperature and lower gravity. Jeff Valenti has suggested that the Mg b wings provide useful constraints on gravity for dwarfs cooler than  $\sim 6200 \text{ K}$ <sup>19</sup>, which is approximately the temperature for 4 of 5 stars we analyze. Fuhrmann et al. (1997) is able to derive an accurate  $\log g$  for Procyon (F5V) from Mg b, so perhaps our concern is unwarranted. Assuming we have derived accurate stellar properties, we find that models fit best with  $\log t = 9.4 \pm 0.05$  (2.25 - 2.8 Gyr), which encompass the error bars of CWW 44.

The models barely pass through the error bars for the G0/2 dwarf (CWW 91), even though this should be the one star of the five we know for certain has broad enough Mg b wings to provide adequate constraint on  $\log g$ , since it is most similar to the Sun. If we assume  $\log g$  is at fault, but  $T_{\text{eff}}$  and  $[\text{Fe}/\text{H}]$  are accurate (this is probably a safe assumption because many more spectral features contribute to the derivation of these parameters), then we can fix  $\log g$  according to the isochrone. Using the Padova isochrone at  $\log t = 9.4$  (2.5 Gyr) and  $[\text{M}/\text{H}] = +0.1$ , we find  $\log g = 4.44$  instead of 4.35, at mass  $M = 1.05 M_{\odot}$ . We queried the  $g'r'i'$  and  $JHK_S$  pho-

<sup>19</sup> <http://www-int.stsci.edu/~valenti/sme.html>



**Table 4**  
Spectroscopic analysis of R147 stars

Property	CWW 44 <sup>a</sup>	CWW 91 <sup>a</sup>	CWW 21 <sup>a</sup>	CWW 22 <sup>a</sup>	CWW 78 <sup>a</sup>	HD 179691 <sup>b</sup>	HD 180112 <sup>b</sup>	HD 180795 <sup>b</sup>
Type	mid-F MSTO	G0/2 V	subgiant	mid-F MSTO / SB1?	late-F V	K1 III	K0 III	K0 III
$T_{\text{eff}}$ (K)	6273 (5)	5747 (62)	6129 (25)	6350 (80)	6115 (52)	4573 (80)	4733 (80)	4658 (80)
$\log g$ (gm cm s <sup>-2</sup> )	4.11 (0.02)	4.35 (0.11)	3.79 (0.07)	3.6 (0.06)	4.27 (0.08)	2.28 (0.15)	2.53 (0.15)	2.43 (0.15)
RV (km s <sup>-1</sup> )	41.41	41.50	40.35	46.63	41.02	46.7	40.1	40.8
$v \sin i$ (km s <sup>-1</sup> )	6.87 (0.69)	0.32 (0.33)	6.50 (0.61)	6.91 (0.73)	6.09 (0.65)	N/A	N/A	N/A
[M/H]	0.07 (0.01)	0.06 (0.03)	0.09 (0.03)	-0.01 (0.04)	-0.11 (0.03)	N/A	N/A	N/A
[Na/H]	0.22 (0.02)	0.23 (0.01)	0.12 (0.01)	-0.02 (0.08)	-0.14 (0.03)	0.24	0.16	0.24
[Si/H]	0.14 (0.01)	0.11 (0.02)	0.10 (0.01)	0.00 (0.03)	0.02 (0.02)	0.08 ± 0.08	0.15 ± 0.06	0.25 ± 0.08
[Ti/H]	0.28 (0.02)	0.16 (0.02)	0.25 (0.03)	0.03 (0.05)	0.06 (0.04)	-0.03 ± 0.07	0.04 ± 0.05	-0.02 ± 0.04
[Fe/H]	0.17 (0.01)	0.11 (0.02)	0.22 (0.01)	0.08 (0.03)	-0.00 (0.02)	N/A	N/A	N/A
[FeI/H]	N/A	N/A	N/A	N/A	N/A	0.03 ± 0.06	0.14 ± 0.06	0.16 ± 0.04
[FeII/H]	N/A	N/A	N/A	N/A	N/A	-0.02 ± 0.09	0.07 ± 0.07	0.08 ± 0.04
[Ni/H]	0.07 (0.01)	0.05 (0.02)	0.13 (0.01)	-0.03 (0.06)	-0.02 (0.03)	-0.04 ± 0.08	0.04 ± 0.06	0.12 ± 0.07
$\chi^2_{\nu}$	2.90	2.86	4.07	5.88	2.18	N/A	N/A	N/A
$\log t$ (years)	N/A	N/A	N/A	N/A	N/A	9.2 ± 0.5	9.0 ± 0.4	9.0 ± 0.4

**Note.** — Rows and SME statistical uncertainties: (Type) Rough Spectral Type, ( $T_{\text{eff}}$ ) Effective Temperature:  $\sigma = 44$  K, ( $\log g$ ) Surface Gravity:  $\sigma = 0.06$  dex, (RV) Radial Velocity ( $v \sin i$ ) projected rotational velocity:  $\sigma = 0.5$  km s<sup>-1</sup>, ([M/H]) Metallicity =  $\log_{10} Z/Z_{\odot}$  ([Na/H] .. [Ni/H]) Sodium, Silicon, Titanium, Iron and Nickel abundance:  $\sigma = 0.03$  dex, ( $\chi^2_{\nu}$ ) Reduced  $\chi^2$  of the fit, ( $\log t$ ) age in years assuming  $d = 280$  pc

<sup>a</sup> Our SME analysis results of Keck/HIRES spectra

<sup>b</sup> Red giants analyzed by Pakhomov et al. (2009), reproduced here for comparison.

tometry from the isochrone and perform a brute force least-squares fit for distance modulus and visual extinction in the range  $m - M = 7 - 8$  and  $A_V = 0 - 0.5$ , with 0.01 mag. step sizes,  $JHK_S$  errors according to 2MASS ( $\sigma = 0.023, 0.026, 0.021$  mag.) and  $g'r'i'$  errors set to  $\sigma = 0.03$  mag. We find a minimum  $\chi^2$  at  $m - M = 7.46 \pm 0.02$ ,  $A_V = 0.22 \pm 0.03$ . (see Figures 15, 16). We perturbed  $[M/H] \pm 0.02$  dex and  $\log t \pm 0.5$ , then re-fit and find uncertainties of 0.04 and 0.01 mag. for  $m - M$  and  $A_V$ . We then perturbed the SME  $T_{\text{eff}}$  by  $\pm 50$ K and re-fit, and find uncertainties of 0.06 and 0.04 mag. for each parameter. Adopting these conservative errors, we find  $m - M = 7.46 \pm 0.06$  and  $A_V = 0.22 \pm 0.04$ .

#### 4.4. Fitting Isochrone Models to Broadband Photometry

Up to this point, we have fit isochrones to a  $T_{\text{eff}} - \log g$  diagram with values derived with SME from Keck spectra of 5 stars. Now we perform a more traditional fit to the broadband optical and NIR photometry of all cluster members, and will find results consistent with our spectroscopic solution. We will see that our preferred model does not well describe the cooler red giants and K dwarfs, and so we will exclude these stars from our final fits presented here and instead focus on the upper FG dwarf main sequence and turnoff (Figures 18, 19).

Naylor & Jeffries (2006) have developed a maximum-likelihood method called  $\tau^2$  for fitting model isochrones to color - magnitude diagrams (see also Naylor 2009)<sup>20</sup>. This method simulates a cluster CMD from an isochrone, with a user-defined binary fraction. The user supplies a star catalog including the color, magnitude, and photometric errors which the  $\tau^2$  code assumes are normally distributed. This method is powerful because it naturally accommodates errors in both color and magnitude, and accounts for the binary sequence. The code performs a grid search across a specified range of distances and ages, for isochrones of a given metallicity and reddening, and identifies best values, confidence intervals, and returns two diagnostics for assessing how well the model describes the data: a reduced- $\tau^2$  (analogous to  $\chi^2_\nu$ ) and a probability value,  $Pr$ .

While the  $\tau^2$  code includes an isochrone library, we make use of the user-supplied isochrone feature and pass it Padova grids (Girardi et al. 2000; Marigo et al. 2008)<sup>21</sup>, which provide models calculated for the CFHT/MegaCam  $g'r'i'z'$  filter set.

The  $\tau^2$  code does not currently solve for  $A_V$ , so we de-redden our catalog before running  $\tau^2$  with the relationships  $A_{g'}/A_V = 1.167$  and  $A_{i'}/A_V = 0.656$  provided by the Padova CMD website<sup>22</sup>. We selected the 56 R147 members of highest confidence ('Y'), excluding the later K dwarfs and red giants with more uncertain theoretical SEDs ( $0.4 < g' - i' < 0.85$  mag.)<sup>23</sup>

<sup>20</sup> code available at <http://www.astro.ex.ac.uk/people/timn/tau-squared/>

<sup>21</sup> models available at <http://stev.oapd.inaf.it/cmd>

<sup>22</sup> for a G2 dwarf, using a Cardelli, Clayton, & Mathis (1989) extinction curve with  $R_V = 3.1$

<sup>23</sup> Dotter et al. (2008) note that the Padova isochrones are hotter and bluer in the later main sequence than other commonly used models including the DSEP (Dartmouth Stellar Evolution Program) and Yale-Yonsei (Y<sup>2</sup>). Also, (VandenBerg et al. 2007) showed that isochrones could not simultaneously fit the M67 optical CMD

We ran  $\tau^2$  for metallicities  $[M/H]$  ranging from Solar to +0.2 ( $Z = 0.030$ , the maximum provided by Padova), and  $A_V = 0.0$  to 0.5 mag. (the upper limit is set by the Schlegel, Finkbeiner, & Davis (1998) dust map). We allowed  $\tau^2$  to search distances ranging from 200 to 400 pc (range suggested by the HIP1 ( $\approx 270$  pc) and HIP2 ( $\approx 220$  pc) parallaxes, plus an extra 130 pc on the far side) and ages 1 to 4 Gyr (step size is 0.01 in  $\log t$ , encompassing the 2.5 Gyr value suggested by our fit to the  $T_{\text{eff}} - \log g$  diagram in Figure 15).

We find high probabilities for a large suite of models, demonstrating the flatness of the  $\tau^2$  space and high degree of degeneracy between age, metallicity, distance and extinction. Figure 17 plots the best distance and age values for a range of extinctions, with metallicity fixed at our spectroscopic value of  $[M/H] = +0.08$ . If we apply the age constraint from the  $T_{\text{eff}} - \log g$  diagram fit (2.25 to 2.7 Gyr, illustrated by the black error bar on the right side of Figure 17), then this restricts distance and extinction to  $m - M = 7.25 - 7.4$  and  $A_V = 0.2 - 0.3$ .

##### 4.4.1. An alternative solution?

Our best isochrone fit in the optical misses the K dwarfs and red giants, and suggests that most of the SB2s are triples. We acknowledge that the majority of the R147 RGB has saturated, and thus unreliable, optical photometry. As noted previously, we also do not expect the Padova models to fit the cooler stars, at least in the optical where uncertain opacities for the metal lines yield poor theoretical SEDs. Despite the mismatch between the cool stars and our optical isochrone solution, we think it is a reliable solution because these features are well fit in the NIR ( $J - K_S$ ) CMD, and the resulting parameters are consistent with the  $T_{\text{eff}} - \log g$  diagram fit.

Nevertheless, we have searched for an isochrone model that fits the major optical CMD morphologies: single and binary main sequences, MSTO, sub giants and red giants.  $\tau^2$  solves for age and distance, but we need to test a range of ages and metallicities because these parameters control the shape of the isochrone, whereas distance and extinction simply translate the isochrone across the color - magnitude space.

In order to efficiently find the  $(m - M) - A_V$  combination that best matches each  $\log t - [M/H]$  isochrone to the  $(g' - i')$  CMD, we use our stellar cluster simulator (§3.2) to map out the CMD locus for each model. We set the photometric error  $\sigma_{g'i'} = 0.01$ ,  $m - M = 7$ ,  $A_V = 0$ , the binary fraction to 50%, and generated  $10^4$  stars. While we included differential extinction in preliminary fits, the results presented below utilized simulations with  $\delta A_V = 0$ , and we note no significant difference in our results. We binned the synthetic cluster CMD into 0.025 mag. pixels, comparable to the photometric error, and binned the 'Y' members in the same fashion, minus the blue stragglers, red giants and K dwarfs. We then computed the 2D cross-correlation between the two distributions. The location of the peak signal in the resulting map provides the shift required to best align the isochrone model to the data.

Although this is not a statistically rigorous method for isochrone fitting, it is conceptually straightforward, simple to code, it can efficiently test hundreds of models in

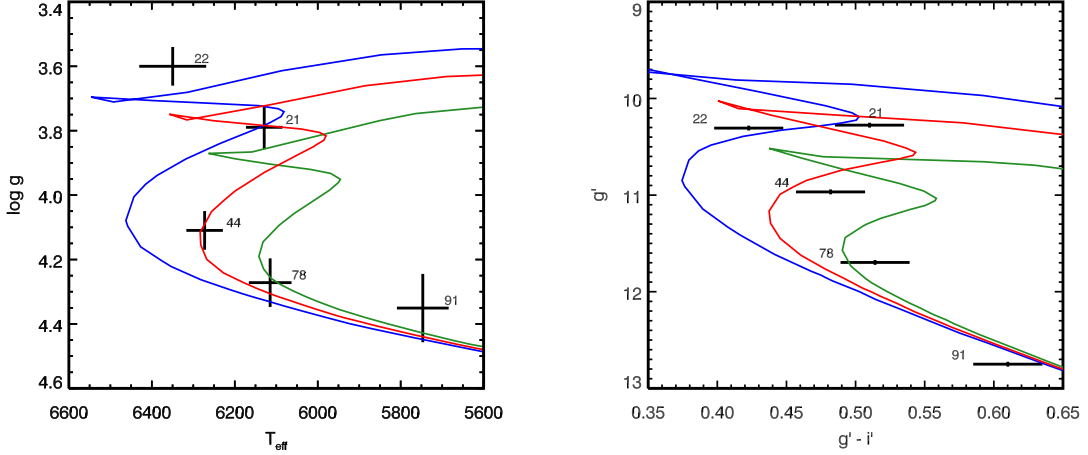


**Figure 15.** Left:  $T_{\text{eff}} - \log g$  diagram of five stars with Keck/HIRES spectra and properties derived with SME. Numbers indicate CWW ID. Padova isochrones overlaid with  $[M/H] = +0.10$  and  $\log t = 9.3$  (blue, 2 Gyr), 9.4 (red, 2.51 Gyr), and 9.5 (green, 3.16 Gyr). Isochrones with ages of 2.34 and 2.7 Gyr encompass the error bars of CWW 44. Right: CFHT/MegaCam ( $g' - i'$ ) CMD for the same five stars, with 0.025 mag. error bars. Padova isochrones of same age and color scheme are overlaid with  $m - M = 7.46$ ,  $A_V = 0.22$ . (see Figure 16)

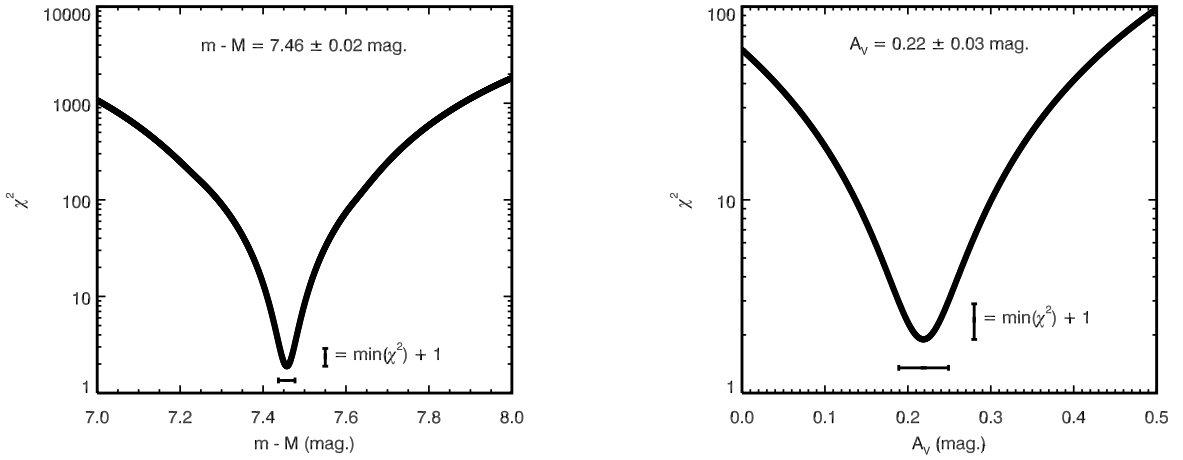


**Figure 16.** Inferring distance and extinction: brute force least squares fit of  $g'r'i'JHK_S$  photometry for CWW 97 to a  $1.05 M_{\odot}$  star with SED drawn from a Padova isochrone with  $\log t = 9.4$  and  $[M/H] = +0.1$  (mass, age and metallicity suggested by SME analysis of a Keck/HIRES spectrum). We calculate  $\chi^2 = \sum (x_i - \mu_i)^2 / \sigma_i^2$ , where  $x_i$  is the measurement,  $\mu_i$  is the model value, and assuming  $\sigma_{g'r'i'} = 0.03$  mag. and  $\sigma_{JHK_S} = 0.025$  mag.  $\chi^2$  is minimized at  $m - M = 7.46 \pm 0.02$  and  $A_V = 0.22 \pm 0.03$ .

an automated fashion to more quickly cover the age – composition parameter space, and it provides a diagnostic for model selection: the model with the maximum cross-correlation signal. Three panels in Figure 18 plot age, distance and extinction versus the cross-correlation signal, normalized to the maximum value, with metallicity fixed at  $[M/H] = +0.08$ . Although broad, there are clear peaks in each diagram. We find the best model is  $\log t = 9.39$ ,  $m - M = 7.35$ ,  $A_V = 0.26$ .

The fourth panel of Figure 18 plots the isochrones (gray) of each solution for  $\log t = 9.0$  to 9.6 (in steps of 0.01). The R147 members used in the fit are plotted in green, and the rest of our membership list is plotted in black. The best model quoted above is overlaid in red. We also plot in blue the model with  $\log t = 9.53$ ,  $[M/H] +0.08$ ,  $m - M = 6.92$ , and  $A_V = 0.11$ . These two mod-

els are also displayed in Figure 19 for both ( $g' - i'$ ) and ( $J - K_S$ ) CMDs. The older (blue) solution is (perhaps naively) attractive because it fits the K dwarfs, MSTO, RGB, and the SB2 sequence (which otherwise we would have to assume are mostly triples or non-members). One weakness is that it overshoots a good deal of the upper main sequence.

If this model is correct, it would require the nearly 20 stars it overshoots to be either less extinguished than the cluster overall by 0.1 – 0.4 mag., which is a problem for a model with  $A_V = 0.1$  because it would imply certain sight lines have negative extinction (a physical impossibility), or require atypically large color errors at  $\sigma > 0.1$  mag., or else the model rejects these stars as non-members. The problem persists in the 2MASS CMD (Figure 19): while it also matches the SB2s to the

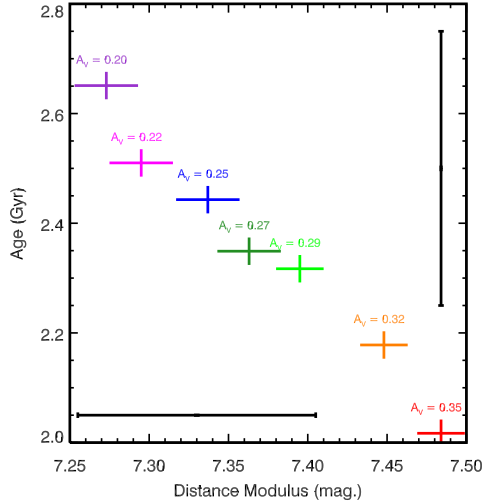


**Figure 17.** This plot illustrates the degeneracy between extinction, age and distance in isochrone fits to broadband photometry. Results are plotted from fitting 7 different  $A_V$  values with  $\tau^2$ , with  $[M/H]$  fixed at +0.08 according to our SME analysis. All fits returned high  $\tau^2$  probabilities, and so model selection is only possible when we place additional constraints from our spectroscopic analysis. In Figure 15, we showed that a 5 star  $T_{\text{eff}} - \log g$  diagram was best fit by a Padova isochrone with age =  $2.5 \pm 0.25$  Gyr, illustrated by the error bar on the right side of this figure. This corresponds to a distance modulus of  $m - M = 7.35 + 0.05 - 0.1$ , shown by the error bar at the bottom of the figure, and  $A_V = 0.25 + 0.08 - 0.05$ .

equal mass binary sequence, it still overshoots on the single mass sequence (blue side, 18 stars), requiring  $\delta A_V = 0.2 - 0.5$  to explain the overshoot with differential reddening.

Furthermore, an age of  $\log t > 9.5$  is prohibited by the  $T_{\text{eff}} - \log g$  fit. Assuming we have derived accurate stellar properties with SME, then we must reject the older fit. If we have good photometry and membership, and R147 does not suffer a large amplitude differential reddening effect, then we must conclude that simultaneously fitting all optical CMD features is not advisable and can deliver (most likely inaccurate) results inconsistent with spectroscopy and NIR photometry, at least for Solar / super-Solar metallicity clusters.

#### 4.4.2. Final Synthesis and Sources of Uncertainty

We have fit Padova isochrone models to three separate datasets: a  $T_{\text{eff}} - \log g$  diagram consisting of 5 stars with values derived from SME, and both optical ( $g' - i'$ ) and NIR ( $J - K_S$ ) CMDs. We have chosen to use the Padova isochrones for our preliminary investigation into the properties of R147 because it provides colors in the MegaCam filter set. Other models (e.g. Dartmouth and Yonsei-Yale) show differences in the main sequence turnoff region, which provides the primary age constraint, and in the lower main sequence, where Padova runs bluer than Dartmouth and Yonsei-Yale. Our results, especially for age, may therefore depend on the model chosen, a possibility we will explore in a more detailed analysis in a future work, where we intend to perform a simultaneous 7-band isochrone fit using our optical  $g'r'i'z'$  photometry, and  $JHK_S$  from

UKIRT.

Our solution is subject to additional sources of uncertainty, including photometric error, unresolved multiple star systems, and the possibility of differential extinction. Main sequence fitting, both to the single star and equal mass binary sequences, provides the primary constraint on the sum of distance and extinction. Ideally, these sequences would be vertically offset by 0.75 magnitudes (or double the brightness), but for R147, there are separations of 1 magnitude or more. This unexpected offset could be explained by differential extinction, which would widen the sequence in both directions, by a population of triple systems, or if the stars are not actually cluster members. In this preliminary investigation, we have not yet untangled this  $\delta A_V$  - multiplicity - membership degeneracy on a star by star basis, but such an analysis would improve the precision of the cluster parameters.

At 315 pc and  $1^\circ.25$  in angular radius, we expect a physical radius of  $\sim 5$  pc, which introduces a differential distance modulus of  $\delta(m - M) = 0.02$  across the cluster. This is comparable to photometric error, and should be part of a more comprehensive error analysis.

In the previous subsections, we presented two plausible solutions: the first has an age  $\sim 2.5$  Gyr, established by an isochrone fit to a spectroscopic  $T_{\text{eff}} - \log g$  diagram, and corroborated by a 2D cross-correlation fit to an optical CMD; the second is much older at  $\sim 3.4$  Gyr. While the older model appears to better match some optical CMD features, and so might be chosen in a *chi-by-eye* fit, it fails in comparison in the NIR CMD and is inconsistent with the spectroscopic results. When only the upper main sequence and turnoff stars are considered, the younger model yields both a larger signal with the 2D cross-correlation technique and a higher  $\tau^2$  probability. We suggest that the Padova isochrones do not well describe the optical SEDs of cool, super-Solar metallicity stars, and attribute this discrepancy to line blanketing and uncertain optical opacities that are difficult to model.

While fitting the fitting the  $T_{\text{eff}} - \log g$  diagram, assuming  $[M/H] = +0.1$ , we find  $\log t = 9.4 \pm 0.03$ , or  $t = 2.5 \pm 0.02$  Gyr. If we increase or decrease the metallicity by  $\pm 0.02$  dex, the age error bars remain similar and the best value for  $\log t$  shifts by 0.02. When we performed the brute force SED fit to the G0/2 dwarf for distance and extinction, we perturbed  $[M/H]$  by  $\pm 0.02$  dex,  $\log t$  by  $\pm 0.5$ , and  $T_{\text{eff}}$  by  $\pm 50$ K, and found  $m - M = 7.46 \pm 0.06$  and  $A_V = 0.22 \pm 0.04$ .

For a given metallicity and extinction,  $\tau^2$  returns typical uncertainties of 40 - 100 Myr in age and 0.03 - 0.05 in distance modulus. Although the  $\tau^2$  code does calculate two diagnostics useful for model selection, the reduced  $\tau^2$  and a probability value, for the range of parameters we searched, the high degree of degeneracy between the four cluster parameters enabled  $\tau^2$  to find solutions which delivered high probabilities ( $>60\%$ ) and reduced  $\tau^2$  values all  $\approx 1$ . Instead, we will select our preferred parameter set by fixing the metallicity according to our spectroscopic SME results:  $[M/H] = +0.08$ , and the age according to the  $T_{\text{eff}} - \log g$  result at 2.5 Gyr. This breaks the degeneracy and we can then accept the corresponding distance and and visual extinction from  $\tau^2$  as best values:  $m - M = 7.33$  ( $d = 292$  pc) and  $A_V = 0.23$ .

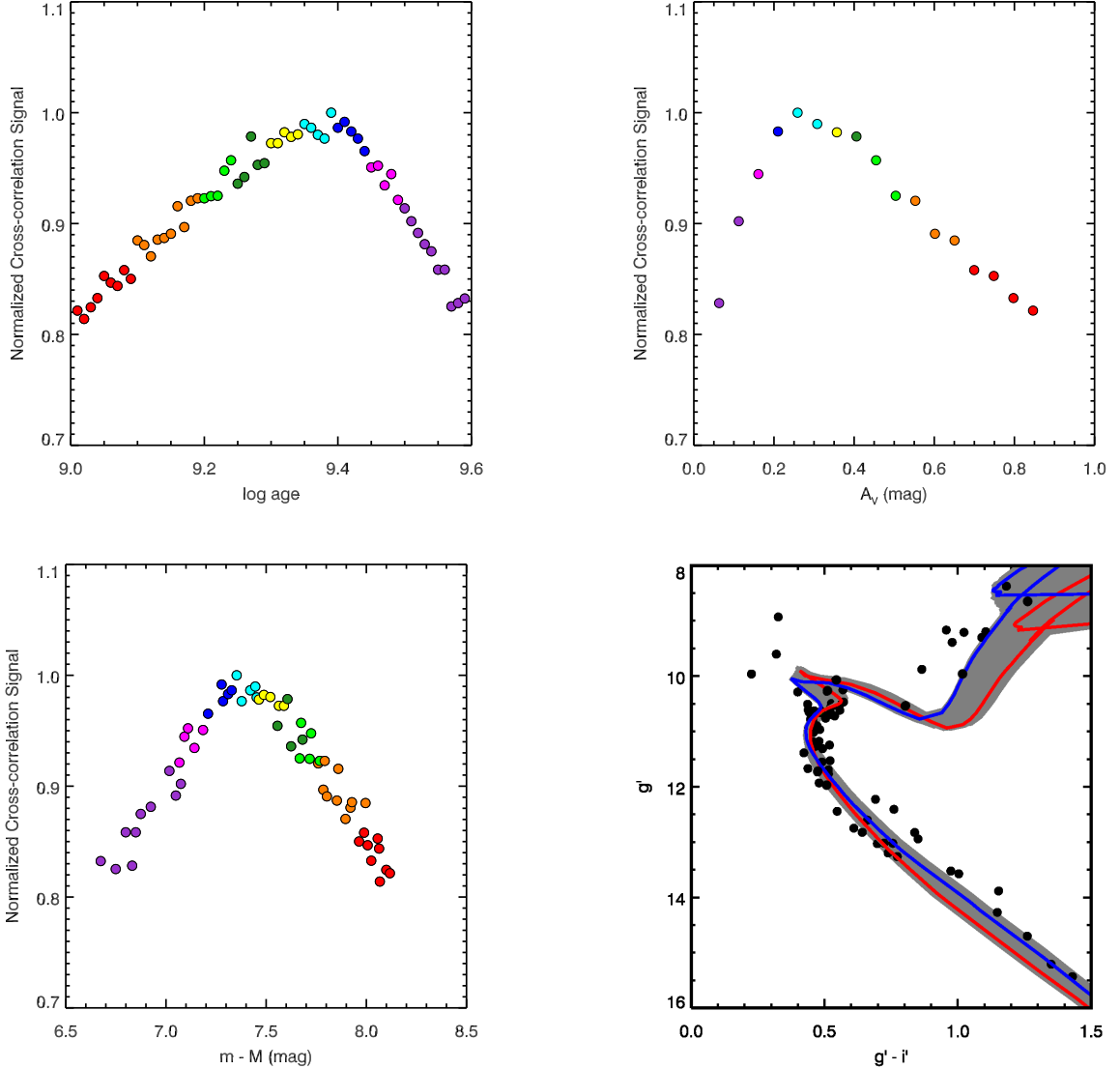


**Figure 18.** Isochrone fitting with 2D cross-correlation method: We tested models with  $\log t = 9.0$  to  $9.6$  (0.01 step size, 1 to 4 Gyr) and  $[M/H] = +0.08$ . Our technique simulates stars clusters with  $10^4$  stars, including binaries and photometric error, and computes the  $m - M$  and  $A_V$  that best matches the R147 photometry. The model with maximum signal in each age / visual extinction / distance modulus bin (0.01, 0.05 mag., 0.025 mag.) is plotted in each panel, color coded according to age. We find that the model with the maximum cross-correlation signal has an age of 2.45 Gyr,  $m - M = 7.35$  and  $A_V = 0.26$ . **Bottom - Right:** This panel plots all solutions in gray with R147 photometry shown as black dots. Two particular models are highlighted: Red -  $\log t = 9.4$ ,  $[M/H] = +0.08$ ,  $m - M = 7.35$  and  $A_V = 0.25$ . Blue -  $\log t = 9.53$ ,  $[M/H] = +0.08$ ,  $m - M = 6.92$  and  $A_V = 0.11$ . While the blue model better matches the K dwarf main sequence, MSTO, and RGB; we think that the red model more likely represents R147 actual properties, because the corresponding fit in NIR ( $J - K_S$ ) is much better (Figure 19) and the model parameters are consistent with our spectroscopic results in §4.3).

This is essentially identical to our 2D cross-correlation results, where we found peak values at an age of 2.5 Gyr,  $m - M = 7.35$  and  $A_V = 0.25$ , for the  $[M/H] = +0.08$  case.

We set our preferred values with generous error bars at age =  $2.5 \pm 0.25$  Gyr ( $\log t = 9.4 \pm 0.03$ ),  $[M/H] = 0.08 \pm 0.03$ ,  $m - M = 7.25$  to  $7.45$  ( $d = 280$  to  $310$  pc), and  $A_V = 0.20$  to  $0.30$ . We set the metallicity error bars according to our SME analysis, ignoring the one anomalously low metallicity result, and the hottest star with a poor  $\chi^2_\nu$  fit. We set the age and error bars according to our fit to the  $T_{\text{eff}} - \log g$  diagram (Figure 15), which is corroborated by the 2D cross-correlation fit (Figure 18). We set the

$A_V$  range and lower bound  $m - M$  value by placing these metallicity and age constraints on our  $\tau^2$  results (Figure 17). We extend the upper bound on  $m - M$  past 7.4 to 7.45 mag. to encompass the result of our SED fit to the G0/2 dwarf. These results are summarized in Table 5, with the values of Kharchenko et al. (2005) and Pakhomov et al. (2009) provided for comparison.

## 5. SUMMARY, DISCUSSION AND UPCOMING WORK

Over 170 years passed since Herschel first cataloged Ruprecht 147 before astronomers finally investigated its properties and membership. Dias, Lépine, & Alessi and Kharchenko et al. demonstrated that a group of 20 – 40

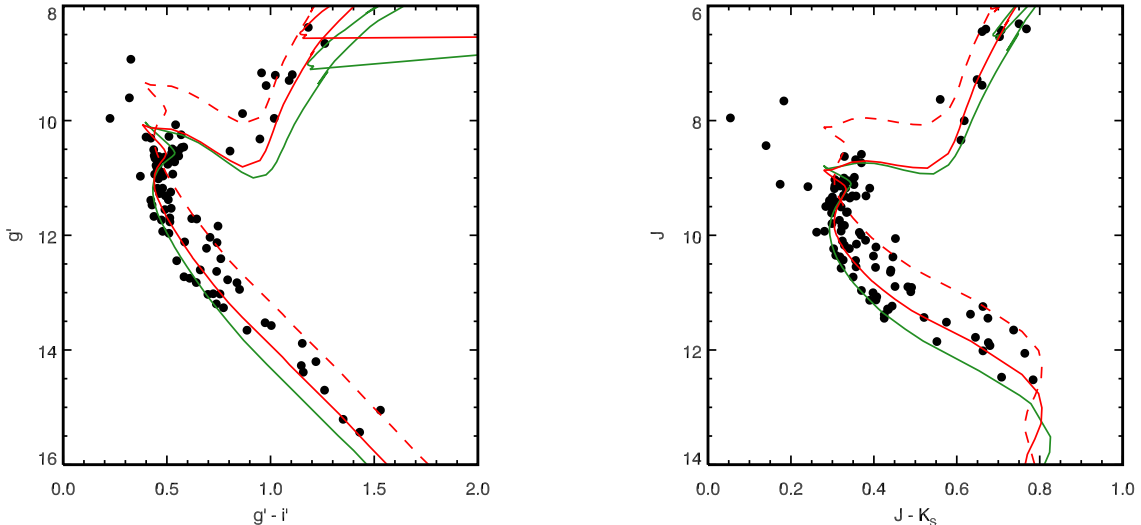


**Figure 19.** Two models from isochrone fitting with 2D cross-correlation method. The green isochrone is our preferred model, with  $\log t = 9.4$ ,  $[M/H] = +0.1$ ,  $m - M = 7.35$  and  $A_V = 0.25$ . The red isochrone is an alternative solution with  $\log t = 9.53$ ,  $[M/H] = +0.1$ ,  $m - M = 6.92$  and  $A_V = 0.11$ , and the dashed line shows the equal mass binary sequence for this model. While the red model better matches the K dwarf main sequence, MSTO, and RGB in the optical; we think the green model more likely represents the actual properties of R147 because it better fits the NIR ( $J - K_S$ ) and is consistent with our spectroscopic results (Figure 15).

**Table 5**  
Table of R147 cluster properties.

$\mu_\alpha$ mas/yr	$\mu_\delta$ mas/yr	$RV^a$ km s $^{-1}$	Age Gyr	Distance pc	$A_V^b$ mag.	Metallicity	Reference
-1.1	-27.3	40.7	$2.51 \pm 0.25$	$295 \pm 15$	$0.25 \pm 0.05$	$[M/H] = +0.08 \pm 0.03$	This work
-0.6	-27.7	41	2.45	175	0.47	N/A	Kharchenko et al. (2005)
N/A	N/A	40.5	$1.26 \pm 1.16$	$280 \pm 100$	0.34	FeI = 0.16, FeII = 0.08	Pakhomov et al. (2009)

**Note.** — Our positions and proper motions are median values for ‘Y’ and ‘P’ members.

<sup>a</sup> Our RV is the average of our two Keck velocities. Kharchenko et al.’s velocity is from Wilson (1953). Pakhomov et al.’s velocity is the average of the two apparent single stars. See Section 3.1.

<sup>b</sup>  $A_V$  assumes a  $R_V = 3.1$  reddening law.

stars at the location of R147 were in fact moving together in the plane of the sky, and estimated this group’s properties, although their analysis was hindered by  $(B - V)$  photometry with a limiting magnitude near the main sequence turnoff. While Kharchenko et al. (2005) was able to determine an age (2.45 Gyr) from the MSTO consistent with the results of our analysis, the  $(B - V)$  main sequence is dominated by photometric error and therefore provides a weak constraint on the distance, which their isochrone fitting has apparently placed 125 pc too close, at 175 pc compared to the 300 pc distance we find here. Nevertheless, these works by Dias, Lépine, & Alessi and Kharchenko et al. are significant because they essentially re-discovered R147. Pakhomov et al. (2009) first spectroscopically determined the composition for 3 red giant members, showing the cluster to be super-Solar (§1.2).

We queried the NOMAD catalog for stars within  $1^\circ.5$  of the cluster center, and out of the 750,000 stars, we find 1348 with proper motion within 5 mas/yr of the R147 value (astrometric values from Kharchenko et al. 2005). We conducted an initial radial velocity survey at Lick and Palomar Observatories and for the first time con-

firm that over 100 stars are likely members of Ruprecht 147 and they are indeed moving together in three dimensions through the Galaxy (§2.2.3, 3.1). We followed up this initial survey with high resolution and signal-to-noise Ca II H & K spectra with MMT/Hectochelle, and used these second epoch RVs, at higher precision, to investigate binarity (§2.5, 3.3.3, 3.3.4). We have imaged the cluster in four optical bands (§2.3), and combined with 2MASS NIR photometry (§3.3.2), used the resulting CMDs to establish a membership list with 86 high-confidence members, 16 possible members, and 4 unlikely members (§3).

We have obtained high-resolution, high-SNR spectra of five members (§2.4), and determine the metallicity to be super-Solar using the SME spectral synthesis code, and find  $[M/H] = +0.08 \pm 0.03$  and zero  $\alpha$ -enhancement (§4.2).

We have fit Padova isochrones to the  $T_{\text{eff}} - \log g$  diagram resulting from our spectroscopic analysis, and find that the age of R147 is best fit by a Padova isochrone with age 2.5 Gyr, enriched at  $[M/H] = +0.1$  (§4.3).  $T_{\text{eff}} - \log g$  diagram isochrone fitting is independent of distance and visual extinction, which makes it a powerful

tool, but this also means it does not directly provide any information on these parameters. We queried the best fit Padova isochrone for a star with  $T_{\text{eff}}$  and  $\log g$  closest to the values for the G0/2 dwarf we derived with SME, then performed a brute force SED fit to the resulting synthetic  $g'r'i'JHK_S$  photometry, and find a minimum  $\chi^2$  at  $m - M = 7.46$  (310 pc) and  $A_V = 0.22$ .

We consulted the dust map of Schlegel, Finkbeiner, & Davis (1998) to set an upper limit on the amount of visual extinction toward R147,  $A_V < 0.5$  (§4.1), then fit Padova isochrones to the  $(g' - i')$  and  $(J - K_S)$  CMDs using the Naylor (2009)  $\tau^2$  maximum-likelihood method (§4.4). We find that without additional constraints from spectroscopy or additional photometric bands, just fitting an optical CMD with isochrone models yields a suite of solutions all with high  $\tau^2$  probabilities, due to the high degree of degeneracy between age, composition, distance and visual extinction. If we break this degeneracy with the spectroscopic metallicity and age, we find  $m - M = 7.33$  and  $A_V = 0.23$  from  $\tau^2$ . While this model appears to match the main morphological features of the NIR CMD (main sequence from K through F, MSTO, subgiant and red giant branches), in the optical the model overshoots the K dwarfs and runs redder than the RGB. We prefer to attribute this discrepancy in the optical to problems with model opacities in cool, super-Solar metallicity stars due to line blanketing.

We also searched for alternative solutions using a 2D cross-correlation technique, and find that an older, closer and less extinguished solution (age = 3.4 Gyr,  $m - M = 7$ ,  $d = 250$  pc,  $A_V = 0.1$ ) better fits the overall R147 optical CMD, but does a poorer job in NIR and is inconsistent with our spectroscopic results (§4.4.1). We also found that the best model derived with this technique corroborates the age we determined from the  $T_{\text{eff}} - \log g$  fit, as well as the distance and extinction corresponding to this age in our  $\tau^2$  fits.

We recognize significant uncertainty in our solution from the unresolved binary population and possibility of differential extinction across this large cluster. These results are also heavily model-dependent.

### 5.1. Discussion and Future Work

The R147 single star main sequence is not well defined, but blends smoothly into what is apparently the binary population. Evidently, R147 has a large binary fraction. The stellar population has encountered nearly 3 Gyr of Galactic gravitational tidal forces. Evaporation of the lightest-mass members should proceed first, as these stars are most easily accelerated to escape velocity. This process preferentially ejects single stars from the cluster, as multiple star systems of similar spectral type have a greater bound mass. The ongoing dynamical evolution of an open cluster tends to increase the binary fraction, and we may be seeing this effect in the R147 main sequence.

Our membership list is top heavy, dominated by F stars (dwarfs, MSTO and subgiants) and red giants, with fewer numbers of G dwarfs, and only a handful of early K dwarfs. This dynamical evolution and evaporation could also explain the paucity of low mass members, and perhaps if any are left, they exist predominantly in multiples. But this can also be explained by observational

bias: the NOMAD and UCAC-3 astrometric catalogs do not go deep enough to identify these stars. Instead, this question will only be settled by deriving precise proper motions for the faint stars in the R147 field, which we intend to do by re-imaging the cluster with MegaCam in the near future.

If we are able to identify single M dwarfs, these will be the only old ( $>1$  Gyr), single cool dwarfs with known ages and compositions bright enough to admit close spectroscopic study. Once the white dwarf population is identified, it will provide an independent age estimate for the cluster and inform studies of white dwarf cooling curves. At 300 pc, chromospheric activity diagnostics are measurable, as is  $L_X$ , and R147 should prove useful for studying the evolution of angular momentum and magnetic activity at intermediate ages.

For these reasons and more, we will continue our efforts to characterize Ruprecht 147 and establish it as a new and important benchmark for stellar astrophysics.

J.L.C. acknowledges support from the National Science Foundation Graduate Research Fellowship Program, the Stephen B. Brumbach graduate fellowship, and the Zacheus Daniel travel grant program. A.W. acknowledges a Hunter R. Rawlings III Cornell Presidential Research Scholarship.

J.T.W. conceived of and oversaw the project, and collected all of the candidate stellar spectra. A.W. and J.T.W. conducted the radial velocity survey at Palomar and Lick and produced the preliminary R147 membership list. J.M.B. conducted the SME analysis. J.A.J. was PI on the program that obtained the optical photometry from CFHT/MegaCam, and also conducted preliminary SME analysis of Lick and Keck spectra to determine the composition of R147 (results are not reported in this work, though they informed this study). J.L.C. and J.T.W. performed the Hectochelle RV survey. J.L.C. was primarily responsible for the writing of the manuscript and the final analysis and synthesis of all data.

We would like to thank Gabor Fűrész and Andrew Szentgyorgyi for assisting the Hectochelle data reduction; Tim Naylor for assisting us with his  $\tau^2$  code; Aaron Dotter for providing access to the Dartmouth isochrones in the CFHT/MegaCam filter; David Monet and Stephen Levine for providing the NOMAD catalog on HDD; James Graham and James Lloyd for supporting this research; and Matthew Muterspaugh for sharing and swapping Lick 3-m time. We would also like to thank all observing staff and telescope operators at MMT/FLWO, CFHT, Lick, Palomar, and Keck; and Geoff Marcy, Andrew Howard and the California Planet Survey observing team for their assistance in acquiring the Keck spectra. Finally, we thank Debra Fischer, Jeff Valenti, Adam Kraus, Steve Saar, Søren Meibom, Andrew West, Kevin Covey, Marcel Agüeros, Suzanne Hawley, Ivan King, Jay Anderson, Jeff Valenti, Bob Mathieu, Ken Janes, and Eric Mamajek for helpful conversations, suggestions, and support.

This work is based on observations obtained with MegaCam, a joint project of CFHT and CEA/DAPNIA, at the Canada-France-Hawaii Telescope (CFHT) which is operated by the National Research Council (NRC) of Canada, the Institut National des Sciences de l'Univers

of the Centre National de la Recherche Scientifique of France, and the University of Hawaii. Observing time was granted by the University of Hawaii Institute for Astronomy TAC. These data were reduced at the TERAPIX data center located at the Institut d'Astrophysique de Paris.

Observations reported here were obtained at the MMT Observatory, a joint facility of the Smithsonian Institution and the University of Arizona. MMT telescope time was granted by NOAO (Project PA-10A-0378, PI J. Wright), through the Telescope System Instrumentation Program (TSIP). TSIP is funded by NSF.

This publication makes use of data products from the Two Micron All Sky Survey, which is a joint project of the University of Massachusetts and the Infrared Processing and Analysis Center/California Institute of Technology, funded by the National Aeronautics and Space Administration and the National Science Foundation.

Some of the data presented herein were obtained at the W.M. Keck Observatory, which is operated as a scientific partnership among the California Institute of Technology, the University of California and the National Aeronautics and Space Administration. The Observatory was made possible by the generous financial support of the W.M. Keck Foundation. The authors wish to recognize and acknowledge the very significant cultural role and reverence that the summit of Mauna Kea has always had within the indigenous Hawaiian community. We are most fortunate to have the opportunity to conduct observations from this mountain.

This research made use of Montage, funded by the National Aeronautics and Space Administration's Earth Science Technology Office, Computation Technologies Project, under Cooperative Agreement Number NCC5-626 between NASA and the California Institute of Technology. Montage is maintained by the NASA/IPAC Infrared Science Archive.

This research made use of the WEBDA database operated at the Institute for Astronomy of the University of Vienna, NASAs Astrophysics Data System Bibliographic Services, and the SIMBAD database and the Vizier catalogue access tool operated at CDS, Strasbourg, France.

*Facilities:* Shane, Hale, MMT, CFHT, Keck:I

#### REFERENCES

- Agüeros, M. A., Covey, K. R., Lemonias, J. J., Law, N. M., Kraus, A., Batalha, N., Bloom, J. S., Cenko, S. B., Kasliwal, M. M., Kulkarni, S. R., Nugent, P. E., Ofek, E. O., Poznanski, D., & Quimby, R. M. 2011, *ApJ*, 740, 110
- Alter, G., Ruprecht, J., & Vanysek, J. 1958. Catalogue of star clusters and associations
- Archinal, B. A., & Hynes, S. J. 2003. Star clusters
- Bertin, E., Mellier, Y., Radovich, M., Missonnier, G., Didelon, P., & Morin, B. 2002, In *Astronomical Data Analysis Software and Systems XI*, D. A. Bohlender, D. Durand, & T. H. Handley, ed., volume 281 of *Astronomical Society of the Pacific Conference Series*, p. 228
- Burnham, R. 1966. *Burnham's celestial handbook; an observer's guide to the universe beyond the solar system. A descriptive catalog and reference handbook of deep-sky wonders for the observer, student, research worker, amateur or professional astronomer.*
- Cardelli, J. A., Clayton, G. C., & Mathis, J. S. 1989, *ApJ*, 345, 245–256
- Dias, W. S., Lépine, J. R. D., & Alessi, B. S. 2001, *A&A*, 376, 441–447
- Dias, W. S., Alessi, B. S., Moitinho, A., & Lépine, J. R. D. 2002, *A&A*, 389, 871–873
- Dias, W. S., Assafin, M., Flório, V., Alessi, B. S., & LÍbero, V. 2006, *A&A*, 446, 949–953
- Dotter, A., Chaboyer, B., Jevremović, D., Kostov, V., Baron, E., & Ferguson, J. W. 2008, *ApJS*, 178, 89–101
- Dreyer, J. L. E. 1888, *MmRAS*, 49, 1–237
- Drimmel, R., & Spergel, D. N. 2001, *ApJ*, 556, 181–202
- Elsanhoury, W. H., Hamdy, M. A., Nouh, M. I., Saad, A. S., & Saad, S. M. 2011, *ISRN Astronomy and Astrophysics*, vol. 2011, id.#127030, 2011
- Fabricant, D., Fata, R. G., McLeod, B. A., Szentgyorgyi, A. H., Barberis, J., Bergner, Jr., H. W., Brown, W. R., Caldwell, N., Conroy, M. A., Eng, R., Epps, H., Furesz, G., Gauron, T. M., Geary, J., Goddard, R. E., Hartmann, L., Hertz, E. N., Honsa, M., Mueller, M., Norton, T. J., Ordway, M. P., Roll, Jr., J. B., Williams, G. G., Freedman-Woods, D. L., & Zajac, J. M. 2004, In *Society of Photo-Optical Instrumentation Engineers (SPIE) Conference Series*, A. F. M. Moorwood & M. Iye, ed., volume 5492 of *Presented at the Society of Photo-Optical Instrumentation Engineers (SPIE) Conference*, pp. 767–778
- Fuhrmann, K., Pfeiffer, M., Frank, C., Reetz, J., & Gehren, T. 1997, *A&A*, 323, 909–922
- Fűrész, G., Szentgyorgyi, A. H., & Meibom, S. 2008, In *Precision Spectroscopy in Astrophysics*, N. C. Santos, L. Pasquini, A. C. M. Correia, & M. Romaniello, ed., pp. 287–290
- Girardi, L., Bressan, A., Bertelli, G., & Chiosi, C. 2000, *A&AS*, 141, 371–383
- Herschel, J. F. W. 1833, *Philosophical Transactions of the Royal Society of London*, 123, 359–505
- Herschel, J. F. W. 1863, *Royal Society of London Proceedings Series I*, 13, 1–3
- Høg, E., Fabricius, C., Makarov, V. V., Urban, S., Corbin, T., Wycoff, G., Bastian, U., Schwekendiek, P., & Wicencac, A. 2000, *A&A*, 355, L27–L30
- Hora, J. L., Luppino, G. A., & Hodapp, K.-W. 1994, In *Society of Photo-Optical Instrumentation Engineers (SPIE) Conference Series*, D. L. Crawford and E. R. Craine, eds., volume 2198 of *Society of Photo-Optical Instrumentation Engineers (SPIE) Conference Series*, pp. 498–503
- Kharchenko, N. V. 2001, *Kinematika i Fizika Nebesnykh Tel*, 17, 409–423
- Kharchenko, N. V., Piskunov, A. E., Röser, S., Schilbach, E., & Scholz, R. 2005, *A&A*, 438, 1163–1173
- Kraus, A. L., & Hillenbrand, L. A. 2007, *AJ*, 134, 2340–2352
- Lallement, R., Welsh, B. Y., Vergely, J. L., Crifo, F., & Sfeir, D. 2003, *A&A*, 411, 447–464
- Landsman, W., Aparicio, J., Bergeron, P., Di Stefano, R., & Stecher, T. P. 1997, *ApJ*, 481, L93
- Lynga, G., & Palous, J. 1987, *A&A*, 188, 35–38
- Marigo, P., Girardi, L., Bressan, A., Groenewegen, M. A. T., Silva, L., & Granato, G. L. 2008, *A&A*, 482, 883–905
- Mathieu, R. D. 1983. The structure, internal kinematics and dynamics of open star clusters. Ph.D. thesis, California Univ., Berkeley.
- Mathieu, R. D., Latham, D. W., & Griffin, R. F. 1990, *AJ*, 100, 1859–1881
- Meibom, S., Barnes, S. A., Latham, D. W., Batalha, N., Borucki, W. J., Koch, D. G., Basri, G., Walkowicz, L. M., Janes, K. A., Jenkins, J., Van Cleve, J., Haas, M. R., Bryson, S. T., Dupree, A. K., Furesz, G., Szentgyorgyi, A. H., Buchhave, L. A., Clarke, B. D., Twicken, J. D., & Quintana, E. V. 2011, *ApJ*, 733, L9
- Mermilliod, J. 1995, In *Information & On-Line Data in Astronomy*, D. Egret & M. A. Albrecht, ed., volume 203 of *Astrophysics and Space Science Library*, pp. 127–138
- Mermilliod, J., & Paunzen, E. 2003, *A&A*, 410, 511–518
- Mink, D. J., Wyatt, W. F., Caldwell, N., Conroy, M. A., Furesz, G., & Tokarz, S. P. 2007, In *Astronomical Data Analysis Software and Systems XVI*, R. A. Shaw, F. Hill, & D. J. Bell, ed., volume 376 of *Astronomical Society of the Pacific Conference Series*, pp. 249–+
- Naylor, T. 2009, *MNRAS*, 399, 432–442
- Naylor, T., & Jeffries, R. D. 2006, *MNRAS*, 373, 1251–1263
- Nidever, D. L., Marcy, G. W., Butler, R. P., Fischer, D. A., & Vogt, S. S. 2002, *ApJS*, 141, 503–522



- Pakhomov, Y. V., Antipova, L. I., Boyarchuk, A. A., Bizyaev, D. V., Zhao, G., & Liang, Y. 2009, *Astronomy Reports*, 53, 660–674
- Peri, M. L. 1995. Asteroseismological Observations of Eta Cassiopeiae A with the Palomar East Arm Echelle Spectrograph. Ph.D. thesis, AA(California Inst. of Tech.)
- Perryman, M. A. C., & ESA 1997. The HIPPARCOS and TYCHO catalogues. Astrometric and photometric star catalogues derived from the ESA HIPPARCOS Space Astrometry Mission, The Hipparcos and Tycho catalogues. Astrometric and photometric star catalogues derived from the ESA Hipparcos Space Astrometry Mission, Publisher: Noordwijk, Netherlands: ESA Publications Division, 1997, Series: ESA SP Series vol no: 1200, ISBN: 9290923997 (set)
- Pichardo, B., Moreno, E., Allen, C., Bedin, L. R., Bellini, A., & Pasquini, L. 2012, *AJ*, 143, 73
- Ruprecht, J. 1966, *Bulletin of the Astronomical Institutes of Czechoslovakia*, 17, 33–+
- Sanders, W. L. 1971, *A&A*, 14, 226–232
- Schilbach, E., Kharchenko, N. V., Piskunov, A. E., Röser, S., & Scholz, R.-D. 2006, *A&A*, 456, 523
- Schlegel, D. J., Finkbeiner, D. P., & Davis, M. 1998, *ApJ*, 500, 525–+
- Skrutskie, M. F., Cutri, R. M., Stiening, R., Weinberg, M. D., Schneider, S., Carpenter, J. M., Beichman, C., Capps, R., Chester, T., Elias, J., Huchra, J., Liebert, J., Lonsdale, C., Monet, D. G., Price, S., Seitzer, P., Jarrett, T., Kirkpatrick, J. D., Gizis, J. E., Howard, E., Evans, T., Fowler, J., Fullmer, L., Hurt, R., Light, R., Kopan, E. L., Marsh, K. A., McCallon, H. L., Tam, R., Van Dyk, S., & Wheelock, S. 2006, *AJ*, 131, 1163–1183
- Soderblom, D. R. 2010, *ARA&A*, 48, 581–629
- Szentgyorgyi, A. H., Cheimets, P., Eng, R., Fabricant, D. G., Geary, J. C., Hartmann, L., Pieri, M. R., & Roll, J. B. 1998, In *Society of Photo-Optical Instrumentation Engineers (SPIE) Conference Series*, S. D’Odorico, ed., volume 3355 of *Society of Photo-Optical Instrumentation Engineers (SPIE) Conference Series*, pp. 242–252
- Thackeray, A. D. 1939, *MNRAS*, 99, 492
- Trumpler, R. J. 1930, *Lick Observatory Bulletin*, 14, 154–188
- Valenti, J. A., & Fischer, D. A. 2005, *ApJS*, 159, 141–166
- Valenti, J. A., & Piskunov, N. 1996, *A&AS*, 118, 595–603
- van Leeuwen, F., ed. 2007a. Hipparcos, the New Reduction of the Raw Data, volume 350 of *Astrophysics and Space Science Library*
- van Leeuwen, F., ed. 2007b. Hipparcos, the New Reduction of the Raw Data, volume 350 of *Astrophysics and Space Science Library*
- VandenBerg, D. A., Gustafsson, B., Edvardsson, B., Eriksson, K., & Ferguson, J. 2007, *ApJ*, 666, L105–L108
- Vogt, S. S. 1987, *PASP*, 99, 1214–1228
- Vogt, S. S., Allen, S. L., Bigelow, B. C., Bresee, L., Brown, B., Cantrall, T., Conrad, A., Couture, M., Delaney, C., Epps, H. W., Hilyard, D., Hilyard, D. F., Horn, E., Jern, N., Kanto, D., Keane, M. J., Kibrick, R. I., Lewis, J. W., Osborne, J., Pardeilhan, G. H., Pfister, T., Ricketts, T., Robinson, L. B., Stover, R. J., Tucker, D., Ward, J., & Wei, M. Z. 1994, In *Proc. SPIE Instrumentation in Astronomy VIII*, David L. Crawford; Eric R. Craine; Eds., Volume 2198, p. 362, pp. 362–+
- Wilson, O. C., & Vainu Bappu, M. K. 1957, *ApJ*, 125, 661–+
- Wilson, R. E. 1953, *Carnegie Institute Washington D.C. Publication*, pp. 0–+
- Wright, J. T., Marcy, G. W., Butler, R. P., & Vogt, S. S. 2004, *ApJS*, 152, 261–295
- Zacharias, N., Monet, D. G., Levine, S. E., Urban, S. E., Gaume, R., & Wycoff, G. L. 2004a, In *Bulletin of the American Astronomical Society*, volume 36 of *Bulletin of the American Astronomical Society*, pp. 1418–+
- Zacharias, N., Urban, S. E., Zacharias, M. I., Wycoff, G. L., Hall, D. M., Monet, D. G., & Rafferty, T. J. 2004b, *AJ*, 127, 3043–3059
- Zacharias, N., Finch, C., Girard, T., Hambly, N., Wycoff, G., Zacharias, M. I., Castillo, D., Corbin, T., Divittorio, M., Dutta, S., Gaume, R., Gauss, S., Germain, M., Hall, D., Hartkopf, W., Hsu, D., Holdenried, E., Makarov, V., Martinez, M., Mason, B., Monet, D., Rafferty, T., Rhodes, A., Siemers, T., Smith, D., Tilleman, T., Urban, S., Wieder, G., Winter, L., & Young, A. 2009, *VizieR Online Data Catalog*, 1315, 0–+
- Zhu, Z. 2009, *Research in Astronomy and Astrophysics*, 9, 1285–1302
- Zombeck, M. 2007. *Handbook of Space Astronomy and Astrophysics: Third Edition*, Cambridge University Press

**Table 6**  
Membership list

CWW ID	2MASS ID	$\mu_{\text{RA}}(\sigma_{\mu})$	$\mu_{\text{Dec}}(\sigma_{\mu})$	$\mu\text{Flag}^{\text{a}}$	$g'$	$g' - i'$	$J^{\text{b}}$	$J - K_S^{\text{b}}$	$\text{RV}_{\text{LP}}$	$\text{RV}_{\text{H}}$	Mem. <sup>c</sup>	MemFlag <sup>d</sup>	Notes <sup>e</sup>
1	19152612-1605571	-1.9 (1.1)	-27.8 (0.6)	NO	8.37	1.18	5.31	0.76	38.5	-	Y	YP-YY	RG
2	19172384-1604243	-2.0 (1.0)	-27.3 (0.7)	NO	8.66	1.26	5.27	0.83	43.4	-	Y	YY-YY	RG
3	19161966-1634094	-0.5 (1.0)	-27.5 (1.2)	NO	8.65	-0.10	8.05	-0.02	-	-	Y	Y-YY	BS
4	19171130-1603082	-0.4 (1.1)	-29.1 (1.0)	NO	9.20	1.10	6.40	0.77	42.7	41.1	Y	YYYYY	RG
5	19164073-1616411	-1.3 (1.3)	-26.4 (1.0)	NO	8.81	-0.04	7.95	0.05	-	-	Y	Y-YY	BS
6	19170343-1703138	-0.5 (1.5)	-28.6 (1.5)	NO	9.21	1.02	6.42	0.71	46.2	-	Y	YY-YY	RG
7	19183747-1712575	0.6 (1.5)	-25.6 (1.5)	NO	-	-	6.41	0.67	42.4	-	Y	YY-Y-	
8	19181439-1641226	1.3 (1.0)	-25.6 (1.0)	NO	8.93	0.33	7.66	0.18	-	-	Y	Y-YY	BS
9	19140272-1554055	-1.3 (1.1)	-25.8 (1.1)	NO	9.30	1.09	6.31	0.75	42.1	-	Y	YY-YY	RG/SB1?
10	19155129-1617591	-1.7 (1.3)	-27.9 (1.1)	NO	9.17	0.96	6.45	0.66	41.4	40.6	Y	YYYYY	RG
11	19180978-1616222	-1.3 (1.3)	-28.4 (1.2)	NO	9.39	0.98	6.54	0.70	44.2	-	Y	YY-YY	RG
12	19164388-1626239	-0.4 (1.2)	-28.7 (1.2)	NO	9.60	0.32	8.44	0.14	-	-	Y	Y-YY	BS
13	19131526-1706210	1.6 (1.3)	-26.1 (0.9)	NO	-	-	7.28	0.65	46.4	-	Y	YY-Y-	
14	19134817-1650059	-1.8 (1.0)	-27.3 (1.0)	U3	9.88	0.87	7.63	0.56	43.6	-	Y	YY-YY	RG
15	19164574-1635226	0.4 (1.2)	-27.0 (1.0)	NO	9.96	1.02	7.38	0.66	46.1	41.4	Y	YYYYY	RG
16	19164823-1611522	-0.2 (1.1)	-27.7 (1.3)	NO	9.96	0.23	9.11	0.17	-	-	Y	Y-YY	BS
17	19165670-1612265	-0.2 (1.1)	-27.2 (1.1)	NO	10.07	0.54	8.59	0.37	44.2	40.6	Y	YYYYY	
18	19193373-1658514	-0.2 (1.6)	-26.0 (2.2)	NO	-	-	8.68	0.36	47.2	-	Y	YP-Y-	
19	19161456-1624071	-0.1 (2.0)	-27.7 (1.6)	NO	10.32	0.95	8.00	0.62	43.8	43.9	P	YYPYY	RG
20	19160865-1611148	-0.7 (1.1)	-29.5 (1.1)	NO	10.25	0.57	8.63	0.33	41.8	41.7	Y	YYYYY	
21	19132220-1645096	-4.2 (1.2)	-26.2 (1.1)	NO	10.28	0.51	8.74	0.37	41.9	-	Y	YY-YY	
22	19172382-1612488	-0.4 (1.7)	-31.5 (1.3)	NO	10.31	0.42	9.26	0.44	-	38.2	P	Y-NYY	BS/SB1?
23	19154269-1633050	1.3 (1.6)	-28.2 (2.0)	U3	11.67	0.44	10.38	0.32	34.7	41.2	Y	YNYYY	SB1?
24	19172865-1633313	0.4 (2.0)	-26.4 (1.4)	NO	10.29	0.40	9.11	0.21	41.8	-	Y	YY-PY	not BS
25	19133648-1548104	-1.7 (1.1)	-27.0 (1.2)	NO	10.53	0.80	8.34	0.61	40.7	-	Y	YY-YY	RG
26	19153282-1620388	1.1 (1.1)	-26.0 (1.2)	NO	10.51	0.44	9.03	0.31	46.1	42.0	Y	YYYYY	
27	19171984-1607383	-3.0 (1.4)	-29.8 (1.7)	NO	10.46	0.58	8.96	0.29	48.3	48.3	P	YPNYY	
28	19152638-1700159	-2.4 (2.2)	-31.0 (2.1)	NO	10.53	0.56	9.08	0.24	43.9	-	Y	YY-YY	
29	19173931-1636348	1.6 (1.4)	-26.2 (1.3)	NO	10.47	0.57	9.00	0.33	41.6	-	Y	YY-YY	
30	19155841-1615258	-0.9 (1.3)	-27.5 (1.3)	NO	10.57	0.52	9.20	0.39	41.4	40.7	Y	YYPY	
31	19195154-1603583	2.3 (1.1)	-25.8 (1.5)	NO	-	-	9.05	0.34	41.7	-	Y	YY-Y-	
32	19151540-1619517	-3.7 (1.3)	-29.7 (3.4)	NO	10.70	0.52	9.30	0.33	45.9	42.2	Y	YYYYY	
33	19181155-1629141	0.1 (1.3)	-25.1 (1.5)	NO	10.66	0.44	9.39	0.29	41.2	-	Y	YY-YY	
34	19165477-1702129	0.4 (2.4)	-30.8 (1.6)	NO	10.63	0.46	9.41	0.31	45.8	-	Y	YY-YY	
35	19163976-1626316	-0.2 (1.5)	-24.7 (1.4)	NO	10.53	0.55	9.10	0.32	45.1	41.1	Y	YYYYY	
36	19153626-1557460	0.2 (1.4)	-28.0 (1.6)	NO	10.49	0.53	9.07	0.31	46.4	41.8	Y	YYYYY	
37	19163344-1607515	-3.3 (2.2)	-26.8 (1.4)	NO	10.64	0.49	9.32	0.36	34.6	41.0	Y	YNYYY	
38	19142651-1606340	-3.4 (1.3)	-27.1 (1.7)	NO	10.66	0.48	9.33	0.41	45.1	41.2	Y	YYPY	
39	19150275-1609405	-3.9 (1.8)	-27.4 (1.7)	NO	10.66	0.52	9.19	0.31	42.7	41.7	Y	YYYYY	
40	19163339-1620215	-3.6 (1.5)	-28.8 (2.2)	NO	10.62	0.56	9.18	0.33	42.1	41.5	Y	YYYYY	
41	19170481-1636526	2.2 (1.4)	-30.1 (3.1)	NO	10.61	0.44	9.33	0.30	45.9	-	Y	YY-YY	
42	19183120-1614421	-3.3 (1.3)	-28.3 (2.7)	NO	10.64	0.45	9.32	0.33	44.6	-	Y	YY-YY	
43	19180054-1636016	1.8 (2.2)	-27.3 (3.0)	NO	10.70	0.46	9.44	0.27	44.9	-	Y	YY-YY	
44	19164495-1717074	-0.4 (2.9)	-25.1 (1.6)	NO	10.97	0.48	9.74	0.32	42.2	-	Y	YY-YY	
45	19150860-1657412	-2.0 (1.5)	-30.3 (1.8)	NO	10.82	0.45	9.50	0.28	45.7	-	Y	YY-YY	
46	19163525-1705075	1.1 (2.9)	-27.4 (1.6)	NO	10.80	0.46	9.52	0.30	45.5	-	Y	YY-YY	
47	19131541-1616123	-3.6 (1.1)	-29.1 (1.4)	NO	10.78	0.45	9.51	0.32	44.5	-	Y	YY-YY	
48	19164662-1619208	-0.7 (1.4)	-28.0 (1.3)	NO	10.72	0.54	9.34	0.37	46.3	42.3	Y	YYYYY	
49	19142907-1549056	-0.4 (1.3)	-26.2 (1.3)	NO	10.76	0.50	9.36	0.36	46.2	-	Y	YY-YY	
50	19162934-1645544	-2.0 (1.9)	-25.8 (2.2)	NO	10.97	0.37	9.80	0.30	47.6	-	P	YP-YP	
51	19163620-1607363	-1.8 (0.9)	-24.7 (4.7)	NO	11.02	0.46	9.12 <sup>f</sup>	0.35	44.9	-	Y	YY-YY	
52	19162169-1609510	-1.6 (1.4)	-28.4 (2.2)	NO	10.90	0.47	9.59	0.34	39.2	40.1	Y	YYYYY	
53	19163231-1611346	-3.3 (1.4)	-28.8 (1.4)	NO	10.93	0.53	9.60	0.33	46.9	45.2	P	YNNYP	
54	19165573-1603220	-2.4 (2.8)	-29.6 (1.5)	NO	11.39	0.42	10.10	0.32	48.9	42.8	Y	YYPY	
55	19160452-1605313	-1.4 (2.1)	-23.4 (2.2)	NO	10.94	0.44	9.61	0.30	45.4	41.8	Y	YYYYY	

Table 6 — Continued

CWW ID	2MASS ID	$\mu_{\text{RA}}(\sigma_{\mu})$	$\mu_{\text{Dec}}(\sigma_{\mu})$	$\mu\text{Flag}^{\text{a}}$	$g'$	$g' - i'$	$J^{\text{b}}$	$J - K_S^{\text{b}}$	$\text{RV}_{\text{LP}}$	$\text{RV}_{\text{H}}$	Mem. <sup>c</sup>	MemFlag <sup>d</sup>	Notes <sup>e</sup>
56	19200522-1535360	-0.4 (1.4)	-23.3 (2.8)	NO	-	-	9.83	0.33	40.7	-	Y	YY-Y-	
57	19170433-1623185	-2.5 (3.0)	-28.8 (1.8)	NO	11.23	0.47	9.93	0.27	41.9	41.8	Y	YYYYY	
58	19172172-1535592	0.9 (2.2)	-25.0 (1.3)	NO	11.27	0.46	9.95	0.36	44.6	-	Y	YY-PY	
59	19151260-1705121	0.8 (2.1)	-30.6 (1.6)	NO	11.18	0.48	9.92	0.24	50.1	-	Y	YP-PY	
60	19114731-1632485	0.2 (1.4)	-26.7 (2.0)	NO	11.31	0.49	10.09	0.38	43.5	-	Y	YY-PY	
61	19145840-1650089	-5.8 (2.5)	-28.7 (1.6)	NO	11.18	0.45	9.93	0.32	42.2	-	Y	PY-YY	
62	19164922-1613222	-0.7 (1.5)	-25.2 (2.4)	NO	11.25	0.52	9.84	0.32	45.0	42.5	Y	YYYYY	
63	19152981-1551047	-1.1 (2.0)	-26.9 (1.5)	NO	11.53	0.52	10.17	0.33	39.7	41.4	Y	YYYYY	
64	19152465-1651222	-2.2 (Inf)	-26.2 (Inf)	NO	11.72	0.64	10.20	0.40	-	-	P	Y-PP	SB2
65	19164440-1615338	-6.0 (Inf)	-25.0 (Inf)	NO	13.88	1.15	11.45	0.68	-	-	Y	P-PY	SB2
66	19150050-1614245	-1.7 (Inf)	-26.6 (Inf)	NO	11.71	0.62	10.15	0.36	-	-	P	Y-YP	SB2
67	19151498-1720177	0.1 (2.4)	-28.4 (1.6)	NO	11.84	0.75	10.08	0.47	34.7	-	N	YN-NN	
68	19180536-1646438	0.0 (Inf)	-22.0 (Inf)	NO	13.57	1.00	11.25	0.67	-	-	Y	P-PY	SB2
69	19161864-1611305	-6.6 (3.2)	-29.4 (3.6)	NO	11.38	0.51	9.99	0.37	42.4	37.2	P	PYNPY	
70	19163827-1625039	-2.2 (3.2)	-27.7 (1.3)	NO	11.47	0.43	10.23	0.30	37.9	38.9	P	PPYY	
71	19154511-1623157	1.6 (3.6)	-27.3 (1.5)	NO	11.93	0.48	10.57	0.32	41.4	41.1	Y	YYYYY	
72	19165800-1614277	-1.4 (1.5)	-35.1 (3.9)	NO	12.04	0.71	10.36	0.40	47.9	46.6	N	PPNYP	SB2
73	19160523-1652561	-3.6 (1.5)	-23.7 (4.3)	NO	11.73	0.47	10.43	0.33	42.5	-	Y	YY-YY	
74	19150925-1552241	-0.2 (1.5)	-28.6 (2.1)	NO	11.55	0.49	10.23	0.34	42.1	42.2	Y	YYYYY	
75	19161121-1621485	2.3 (2.7)	-25.0 (2.6)	NO	13.20	0.74	11.43	0.52	39.5	42.2	Y	YYYYY	
76	19134334-1649109	-2.4 (1.2)	-37.6 (1.3)	U3	12.69	0.68	11.13	0.41	43.5	-	P	NY-YY	
77	19150012-1605517	-0.7 (2.5)	-26.4 (2.5)	NO	12.12	0.59	10.56	0.40	50.5	52.6	N	YNNYY	
78	19160879-1524279	-3.7 (1.4)	-27.3 (1.7)	NO	11.70	0.51	10.35	0.31	40.8	-	Y	YY-YY	
79	19142816-1620023	-3.3 (2.4)	-29.6 (2.4)	NO	12.60	0.66	11.00	0.40	42.3	42.1	Y	YYYYY	
80	19162501-1632018	-1.7 (1.5)	-28.7 (4.3)	NO	12.13	0.74	10.38	0.45	41.5	-	P	YY-PP	
81	19151897-1639244	-2.2 (3.2)	-25.0 (2.7)	NO	11.77	0.51	10.44	0.36	41.2	-	Y	YY-YY	
82	19152406-1621519	-1.7 (1.6)	-29.4 (1.5)	NO	11.97	0.51	10.55	0.36	47.9	42.5	Y	PPYY	
83	19134126-1610201	-2.7 (2.5)	-27.7 (2.4)	NO	12.23	0.69	10.64	0.44	42.0	-	Y	YY-YY	
84	19141294-1554291	-2.5 (2.5)	-24.7 (2.5)	NO	12.41	0.76	10.61	0.44	46.7	-	Y	YY-YY	
85	19165940-1635271	0.7 (2.5)	-29.3 (2.5)	NO	12.82	0.64	11.23	0.44	42.6	42.9	Y	YYYYY	
86	19160589-1629481	0.1 (2.6)	-27.4 (2.6)	NO	12.94	0.85	10.98	0.49	44.7	41.6	Y	YYYYY	
87	19160785-1610360	-3.3 (2.7)	-27.5 (2.6)	NO	12.83	0.84	10.91	0.49	45.0	42.4	Y	YYYYY	
88	19162477-1710375	0.0 (2.0)	-32.0 (6.0)	NO	13.02	0.72	11.28	0.43	47.0	-	Y	YY-YY	
89	19173402-1652177	-1.7 (3.3)	-19.6 (4.2)	U3	12.72	0.58	11.07	0.41	47.3	-	P	PP-YY	
90	19163672-1713101	-2.7 (1.6)	-26.1 (4.1)	NO	12.44	0.55	10.95	0.32	42.0	-	Y	YY-YY	
91	19164725-1604093	-0.7 (2.4)	-26.8 (2.4)	NO	12.75	0.61	11.13	0.36	42.8	42.2	Y	YYYYY	
92	19164417-1612222	-1.4 (2.6)	-29.0 (2.6)	NO	12.63	0.74	10.89	0.45	45.1	25.2	P	YNNYY	SB1?
93	19162203-1546159	1.1 (2.5)	-24.8 (2.5)	NO	13.02	0.76	11.29	0.43	41.8	41.7	Y	YYYYY	
94	19152141-1600107	-0.7 (2.5)	-27.6 (2.5)	NO	13.26	0.77	11.43	0.38	43.5	42.8	Y	YYYPY	
95	19170128-1609423	-1.7 (2.5)	-27.2 (2.4)	NO	12.78	0.79	10.90	0.48	40.6	39.1	P	YYPY	
96	19151156-1726308	0.5 (1.5)	-26.0 (1.5)	NO	-	-	10.73	0.35	40.8	-	Y	YY-Y-	
97	19170285-1605166	-1.8 (2.5)	-26.4 (2.4)	NO	13.03	0.70	11.38	0.43	40.9	41.1	Y	YYYYY	
98	19162656-1614545	-3.7 (2.5)	-28.2 (2.5)	NO	13.52	0.97	11.38	0.63	43.2	40.7	Y	YYYPY	
99	19161757-1600177	-3.6 (2.7)	-28.6 (2.6)	NO	13.66	0.89	11.52	0.58	44.8	44.6	P	YNNYY	
100	19145199-1541379	-0.9 (7.6)	-20.5 (7.6)	NO	14.20	1.22	11.67	0.79	42.2	-	P	PY-PY	
101	19153354-1625368	-4.3 (5.8)	-29.3 (2.9)	U3	15.43	1.43	12.52	0.78	46.3	40.5	Y	YYYYY	
102	19124958-1550340	4.0 (4.0)	-26.0 (6.0)	NO	-	-	11.85	0.55	44.3	-	Y	PY-Y-	
103	19134512-1619340	0.5 (7.6)	-21.3 (7.6)	NO	14.27	1.15	11.92	0.68	45.0	-	Y	PY-YY	
104	19193779-1618312	9.1 (7.7)	-8.6 (7.7)	AK	-	-	11.78	0.65	52.4	-	N	NN-Y-	
105	19181352-1614496	0.0 (3.0)	-36.0 (8.0)	NO	14.39	1.16	11.87	0.68	50.5	-	P	NN-YY	
106	19163680-1623032	-5.6 (7.9)	-22.5 (7.7)	NO	15.05	1.53	12.06	0.76	49.3	46.5	P	PPNYY	
107	19163732-1600050	-4.2 (3.1)	-27.5 (3.1)	AK	14.70	1.26	12.02	0.66	42.5	42.1	Y	YYYYY	
108	19172940-1611577	-4.0 (7.0)	-22.0 (4.0)	NO	15.21	1.35	12.47	0.71	48.6	42.8	Y	PPYY	

Table 6 — Continued

CWW ID	2MASS ID	$\mu_{\text{RA}}(\sigma_{\mu})$	$\mu_{\text{Dec}}(\sigma_{\mu})$	$\mu\text{Flag}^{\text{a}}$	$g'$	$g' - i'$	$J^{\text{b}}$	$J - K_S^{\text{b}}$	$\text{RV}_{\text{LP}}$	$\text{RV}_{\text{H}}$	Mem. <sup>c</sup>	MemFlag <sup>d</sup>	Notes <sup>e</sup>
--------	----------	---------------------------------	----------------------------------	-----------------------------	------	-----------	----------------	----------------------	-------------------------	------------------------	-------------------	----------------------	--------------------

**Note.** — Column Notes: (1) CWW ID – This work’s star identification scheme, sorted by  $V$  magnitude. CWW = Curtis, Wolfgang and Wright. (2) 2MASS ID, also provides RA and Dec positions (3, 4) RA and Dec proper motions in mas/yr (5) proper motion reference: NO = NOMAD, U3 = UCAC-3, AK = Adam Kraus (private comm.) (6) CFHT/MegaCam  $g'$  mag. (7)  $g' - i'$  mag. (8) 2MASS  $J$  mag. (9) 2MASS  $J - K_S$  mag. (10) Lick / Palomar RV in  $\text{km s}^{-1}$  (11) Hectochelle RV in  $\text{km s}^{-1}$  (12) Membership probabilities (13) Membership probabilities for each criterion (14) Notes for individual stars. Values in parenthesis are measurement errors.

<sup>a</sup> Proper Motion Reference: NO = NOMAD, U3 = UCAC-3, AK = Adam Kraus (private comm.)

<sup>b</sup> We use 2MASS aperture photometry instead of the default PSF photometry for 18 stars, based on our analysis that these stars, and only these stars, shift position on the  $(J - K_S)$  CMD and that they all move toward the cluster locus. No neighbors are resolved in our optical imaging within  $5''$ . The stars are CWW 22, 24, 27, 28, 30, 37, 38, 43, 48, 49, 57, 59, 67, 68, 90, 91, 94, and 100.

<sup>c</sup> Membership Probability: Y = yes, highest confidence member, P = possible / probable member, N = not likely / non-member

<sup>d</sup> Membership Criteria: proper motion radial distance from cluster value; Lick / Palomar RV, Hectochelle RV, 2MASS  $(J - K_S)$  CMD, CFHT/MegaCam  $(g' - i')$  CMD. Confidence intervals defined in Table 3. A dash ‘-’ indicates no data.

<sup>e</sup> Notes: BS = blue straggler, RG = red giant, SB2 = spectroscopic double line binary, SB1? = inconsistent RVs between multiple epochs

<sup>f</sup> Our MegaCam imaging shows CWW 51 is an optical double, with a star  $1.65''$  away with a similar  $g'r'i'z'$  SED. This double was not resolved in the 2MASS Point Source Catalog. Adding  $0.75$  mag. to the  $J$  band magnitude (halving the brightness, to reflect just the one star) moves CWW 51 in the  $(J - K_S)$  CMD to its neighbors in the  $(g' - i')$  CMD. Despite this realization, we quote the 2MASS PSC photometry here. See §3.3.2.